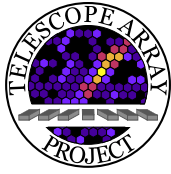


Pierre Auger Observatory and Telescope Array: Joint Contributions to the 35th International Cosmic Ray Conference (ICRC 2017)

The Telescope Array Collaboration



R.U. Abbasi¹, M. Abe², T. Abu-Zayyad¹, M. Allen¹, R. Azuma³, E. Barcikowski¹, J.W. Belz¹, D.R. Bergman¹, S.A. Blake¹, R. Cady¹, B.G. Cheon⁴, J. Chiba⁵, M. Chikawa⁶, A. Di Matteo²⁹, T. Fujii⁷, M. Fukushima^{7,8}, G. Furlich¹, T. Goto⁹, W. Hanlon¹, M. Hayashi¹⁰, Y. Hayashi⁹, N. Hayashida¹¹, K. Hibino¹¹, K. Honda¹², D. Ikeda⁷, N. Inoue², T. Ishii¹², R. Ishimori³, H. Ito¹³, D. Ivanov¹, C.C.H. Jui¹, K. Kadota¹⁴, F. Kakimoto³, O. Kalashev¹⁵, K. Kasahara¹⁶, H. Kawai¹⁷, S. Kawakami⁹, S. Kawana², K. Kawata⁷, E. Kido⁷, H.B. Kim⁴, J.H. Kim¹, J.H. Kim¹⁸, S. Kishigami⁹, S. Kitamura³, Y. Kitamura³, V. Kuzmin^{15†}, M. Kuznetsov¹⁵, Y.J. Kwon¹⁹, B. Lubsandorzhiev¹⁵, J.P. Lundquist¹, K. Machida¹², K. Martens⁸, T. Matsuyama⁹, J.N. Matthews¹, M. Minamino⁹, K. Mukai¹², I. Myers¹, K. Nagasawa², S. Nagataki¹³, T. Nakamura²¹, T. Nonaka⁷, A. Nozato⁶, S. Ogio⁹, J. Ogura³, M. Ohnishi⁷, H. Ohoka⁷, T. Okuda²², M. Ono¹³, R. Onogi⁹, A. Oshima⁹, S. Ozawa¹⁶, I.H. Park²³, M.S. Pshirkov^{15,24}, D.C. Rodriguez¹, G. Rubtsov¹⁵, D. Ryu¹⁸, H. Sagawa⁷, K. Saito⁷, Y. Saito²⁵, N. Sakaki⁷, N. Sakurai⁹, L.M. Scott²⁶, K. Sekino⁷, P.D. Shah¹, T. Shibata⁷, F. Shibata¹², H. Shimodaira⁷, B.K. Shin⁹, H.S. Shin⁷, J.D. Smith¹, P. Sokolsky¹, B.T. Stokes¹, S.R. Stratton^{1,26}, T.A. Stroman¹, T. Suzawa², Y. Takahashi⁹, M. Takamura⁵, M. Takeda⁷, R. Takeishi⁷, A. Taketa²⁷, M. Takita⁷, Y. Tameda¹¹, M. Tanaka²⁰, K. Tanaka²⁸, H. Tanaka⁹, S.B. Thomas¹, G.B. Thomson¹, P. Tinyakov^{15,29}, I. Tkachev¹⁵, H. Tokuno³, T. Tomida²⁵, S. Troitsky¹⁵, Y. Tsunesada³, K. Tsutsumi³, Y. Uchihori³⁰, S. Udo¹¹, F. Urban^{24,31}, T. Wong¹, R. Yamane⁹, H. Yamaoka²⁰, K. Yamazaki²⁷, J. Yang³², K. Yashiro⁵, Y. Yoneda⁹, S. Yoshida¹⁷, H. Yoshii³³, Y. Zhezher¹⁵, Z. Zundel¹

———— • ————

- ¹ High Energy Astrophysics Institute and Department of Physics and Astronomy, University of Utah, Salt Lake City, Utah, USA
- ² The Graduate School of Science and Engineering, Saitama University, Saitama, Saitama, Japan
- ³ Graduate School of Science and Engineering, Tokyo Institute of Technology, Meguro, Tokyo, Japan
- ⁴ Department of Physics and The Research Institute of Natural Science, Hanyang University, Seongdong-gu, Seoul, Korea
- ⁵ Department of Physics, Tokyo University of Science, Noda, Chiba, Japan
- ⁶ Department of Physics, Kinki University, Higashi Osaka, Osaka, Japan
- ⁷ Institute for Cosmic Ray Research, University of Tokyo, Kashiwa, Chiba, Japan
- ⁸ Kavli Institute for the Physics and Mathematics of the Universe (WPI), Todai Institutes for Advanced Study, the University of Tokyo, Kashiwa, Chiba, Japan
- ⁹ Graduate School of Science, Osaka City University, Osaka, Osaka, Japan
- ¹⁰ Information Engineering Graduate School of Science and Technology, Shinshu University, Nagano, Nagano, Japan
- ¹¹ Faculty of Engineering, Kanagawa University, Yokohama, Kanagawa, Japan

- ¹² Interdisciplinary Graduate School of Medicine and Engineering, University of Yamanashi, Kofu, Yamanashi, Japan
- ¹³ Astrophysical Big Bang Laboratory, RIKEN, Wako, Saitama, Japan
- ¹⁴ Department of Physics, Tokyo City University, Setagaya-ku, Tokyo, Japan
- ¹⁵ Institute for Nuclear Research of the Russian Academy of Sciences, Moscow, Russia
- ¹⁶ Advanced Research Institute for Science and Engineering, Waseda University, Shinjuku-ku, Tokyo, Japan
- ¹⁷ Department of Physics, Chiba University, Chiba, Chiba, Japan
- ¹⁸ Department of Physics, School of Natural Sciences, Ulsan National Institute of Science and Technology, UNIST-gil, Ulsan, Korea
- ¹⁹ Department of Physics, Yonsei University, Seodaemun-gu, Seoul, Korea
- ²⁰ Institute of Particle and Nuclear Studies, KEK, Tsukuba, Ibaraki, Japan
- ²¹ Faculty of Science, Kochi University, Kochi, Kochi, Japan
- ²² Department of Physical Sciences, Ritsumeikan University, Kusatsu, Shiga, Japan
- ²³ Department of Physics, Sungkyunkwan University, Jang-an-gu, Suwon, Korea
- ²⁴ Sternberg Astronomical Institute, Moscow M.V. Lomonosov State University, Moscow, Russia
- ²⁵ Academic Assembly School of Science and Technology Institute of Engineering, Shinshu University, Nagano, Nagano, Japan
- ²⁶ Department of Physics and Astronomy, Rutgers University - The State University of New Jersey, Piscataway, New Jersey, USA
- ²⁷ Earthquake Research Institute, University of Tokyo, Bunkyo-ku, Tokyo, Japan
- ²⁸ Graduate School of Information Sciences, Hiroshima City University, Hiroshima, Hiroshima, Japan
- ²⁹ Service de Physique Théorique, Université Libre de Bruxelles, Brussels, Belgium
- ³⁰ National Institute of Radiological Science, Chiba, Chiba, Japan
- ³¹ National Institute of Chemical Physics and Biophysics, Estonia
- ³² Department of Physics and Institute for the Early Universe, Ewha Womans University, Seodaemun-gu, Seoul, Korea
- ³³ Department of Physics, Ehime University, Matsuyama, Ehime, Japan

[†] Deceased

The Pierre Auger Collaboration



PIERRE
AUGER
OBSERVATORY

A. Aab⁷⁷, P. Abreu⁶⁹, M. Aglietta^{50,49}, I.F.M. Albuquerque¹⁸, I. Allekotte¹, A. Almela^{8,11}, J. Alvarez Castillo⁶⁵, J. Alvarez-Muñiz⁷⁶, G.A. Anastasi^{41,43}, L. Anchordoqui⁸³, B. Andrada⁸, S. Andringa⁶⁹, C. Aramo⁴⁷, N. Arsene⁷¹, H. Asorey^{1,27}, P. Assis⁶⁹, J. Aublin³², G. Avila^{9,10}, A.M. Badescu⁷², A. Balaceanu⁷⁰, F. Barbato⁵⁷, R.J. Barreira Luz⁶⁹, K.H. Becker³⁴, J.A. Bellido¹², C. Berat³³, M.E. Bertaina^{59,49}, X. Bertou¹, P.L. Biermann^b, J. Biteau³¹, S.G. Blaess¹², A. Blanco⁶⁹, J. Blazek²⁹, C. Bleve^{53,45}, M. Boháčová²⁹, D. Boncioli^{43,8}, C. Bonifazi²⁴, N. Borodai⁶⁶, A.M. Botti^{8,36}, J. Brack^f, I. Brancus⁷⁰, T. Bretz³⁸, A. Bridgeman³⁵, F.L. Briechele³⁸, P. Buchholz⁴⁰, A. Bueno⁷⁵, S. Buitink⁷⁷, M. Buscemi^{55,44}, K.S. Caballero-Mora⁶³, B. Caccianiga⁴⁶, L. Caccianiga⁵⁶, A. Cancio^{11,8}, F. Canfora⁷⁷, L. Caramete⁷¹, R. Caruso^{55,44}, A. Castellina^{50,49}, F. Catalani¹⁶, G. Cataldi⁴⁵, L. Cazon⁶⁹, A.G. Chavez⁶⁴, J.A. Chinellato¹⁹, J. Chudoba²⁹, R.W. Clay¹², A. Cobos⁸, R. Colalillo^{57,47}, A. Coleman⁸⁷, L. Collica⁴⁹, M.R. Coluccia^{53,45}, R. Conceição⁶⁹, G. Consolati⁴⁶, G. Consolati^{46,51}, F. Contreras^{9,10}, M.J. Cooper¹², S. Coutu⁸⁷, C.E. Covault⁸¹, J. Cronin^{88†}, S. D'Amico^{52,45}, B. Daniel¹⁹, S. Dasso^{5,3}, K. Daumiller³⁶, B.R. Dawson¹², R.M. de Almeida²⁶, S.J. de Jong^{77,79}, G. De Mauro⁷⁷, J.R.T. de Mello Neto^{24,25}, I. De Mitri^{53,45}, J. de Oliveira²⁶, V. de Souza¹⁷, J. Debatin³⁵, O. Deligny³¹, M.L. Díaz Castro¹⁹, F. Diogo⁶⁹, C. Dobrigkeit¹⁹, J.C. D'Olivo⁶⁵, Q. Dorosti⁴⁰, R.C. dos Anjos²³, M.T. Dova⁴, A. Dundovic³⁹, J. Ebr²⁹, R. Engel³⁶, M. Erdmann³⁸, M. Erfani⁴⁰, C.O. Escobar^e, J. Espadana¹⁶⁹, A. Etchegoyen^{8,11}, H. Falcke^{77,80,79}, J. Farmer⁸⁸, G. Farrar⁸⁵, A.C. Fauth¹⁹, N. Fazzini^e, F. Fenu^{59,49}, B. Fick⁸⁴, J.M. Figueira⁸, A. Filipčić^{74,73}, M.M. Freire⁶, T. Fujii⁸⁸, A. Fuster^{8,11}, R. Gaïor³², B. García⁷, F. Gaté^d, H. Gemmeke³⁷, A. Gherghel-Lascu⁷⁰, P.L. Ghia³¹, U. Giaccari²⁴, M. Giammarchi⁴⁶, M. Giller⁶⁷, D. Glas⁶⁸, C. Glaser³⁸, G. Golup¹, M. Gómez Berisso¹, P.F. Gómez Vitale^{9,10}, N. González^{8,36}, A. Gorgi^{50,49}, A.F. Grillo⁴³, T.D. Grubb¹², F. Guarino^{57,47}, G.P. Guedes²⁰, R. Halliday⁸¹, M.R. Hampel⁸, P. Hansen⁴, D. Harari¹, T.A. Harrison¹², A. Haungs³⁶, T. Hebbeker³⁸, D. Heck³⁶, P. Heimann⁴⁰, A.E. Herve³⁵, G.C. Hill¹², C. Hojvat^e, E. Holt^{36,8}, P. Homola⁶⁶, J.R. Hörandel^{77,79}, P. Horvath³⁰, M. Hrabovský³⁰, T. Huege³⁶, J. Hulsman^{8,36}, A. Insolia^{55,44}, P.G. Isar⁷¹, I. Jandt³⁴, J.A. Johnsen⁸², M. Josebachuili⁸, J. Jurysek²⁹, A. Kääpä³⁴, O. Kambeitz³⁵, K.H. Kampert³⁴, B. Keilhauer³⁶, N. Kemmerich¹⁸, E. Kemp¹⁹, J. Kemp³⁸, R.M. Kieckhafer⁸⁴, H.O. Klages³⁶, M. Kleifges³⁷, J. Kleinfeller⁹, R. Krause³⁸, N. Krohm³⁴, D. Kuempel³⁴, G. Kukec Mezek⁷³, N. Kunka³⁷, A. Kuotb Awad³⁵, B.L. Lago¹⁵, D. LaHurd⁸¹, R.G. Lang¹⁷, M. Lauscher³⁸, R. Legumina⁶⁷, M.A. Leigui de Oliveira²², A. Letessier-Selvon³², I. Lhenry-Yvon³¹, K. Link³⁵, D. Lo Presti⁵⁵, L. Lopes⁶⁹, R. López⁶⁰, A. López Casado⁷⁶, R. Lorek⁸¹, Q. Luce³¹, A. Lucero^{8,11}, M. Malacari⁸⁸, M. Mallamaci^{56,46}, D. Mandat²⁹, P. Mantsch^e, A.G. Mariazzi⁴, I.C. Mariş¹³, G. Marsella^{53,45}, D. Martello^{53,45}, H. Martinez⁶¹, O. Martínez Bravo⁶⁰, J.J. Masías Meza³, H.J. Mathes³⁶, S. Mathys³⁴, G. Matthiae^{58,48}, E. Mayotte³⁴, P.O. Mazur^e, C. Medina⁸², G. Medina-Tanco⁶⁵, D. Melo⁸, A. Menshikov³⁷, K.-D. Merenda⁸², S. Michal³⁰, M.I. Micheletti⁶, L. Middendorf³⁸, L. Miramonti^{56,46}, B. Mitrica⁷⁰, D. Mockler³⁵, S. Mollerach¹, F. Montanet³³, C. Morello^{50,49}, G. Morlino^{41,43}, M. Mostafá⁸⁷, A.L. Müller^{8,36}, G. Müller³⁸, M.A. Muller^{19,21}, S. Müller^{35,8}, R. Mussa⁴⁹, I. Naranjo¹, L. Nellen⁶⁵, P.H. Nguyen¹², M. Niculescu-Oglinazu⁷⁰, M. Niechciol⁴⁰, L. Niemietz³⁴, T. Niggemann³⁸, D. Nitz⁸⁴, D. Nosek²⁸, V. Novotny²⁸, L. Nožka³⁰, L.A. Núñez²⁷, L. Ochilo⁴⁰, F. Oikonomou⁸⁷, A. Olinto⁸⁸, M. Palatka²⁹, J. Pallotta², P. Papenbreer³⁴, G. Parente⁷⁶, A. Parra⁶⁰, T. Paul⁸³, M. Pech²⁹, F. Pedreira⁷⁶, J. Pekala⁶⁶, R. Pelayo⁶², J. Peña-Rodríguez²⁷, L. A. S. Pereira¹⁹, M. Perlin⁸, L. Perrone^{53,45}, C. Peters³⁸, S. Petrera^{41,43}, J. Phuntsok⁸⁷, R. Piegaia³, T. Pierog³⁶, M. Pimenta⁶⁹, V. Pirronello^{55,44}, M. Platino⁸, M. Plum³⁸, J. Poh⁸⁸, C. Porowski⁶⁶, R.R. Prado¹⁷, P. Privitera⁸⁸, M. Prouza²⁹, E.J. Quel², S. Querschfeld³⁴, S. Quinn⁸¹, R. Ramos-Pollan²⁷, J. Rautenberg³⁴, D. Ravignani⁸, J. Ridky²⁹, F. Riehn⁶⁹, M. Risse⁴⁰, P. Ristori², V. Rizi^{54,43}, W. Rodrigues de Carvalho¹⁸, G. Rodriguez Fernandez^{58,48}, J. Rodriguez Rojo⁹, M.J. Roncoroni⁸, M. Roth³⁶, E. Roulet¹, A.C. Rovero⁵, P. Ruehl⁴⁰, S.J. Saffi¹², A. Saftoiu⁷⁰, F. Salamida^{54,43}, H. Salazar⁶⁰, A. Saleh⁷³, G. Salina⁴⁸, F. Sánchez⁸, P. Sanchez-Lucas⁷⁵, E.M. Santos¹⁸, E. Santos⁸, F. Sarazin⁸², R. Sarmiento⁶⁹, C. Sarmiento-Cano⁸, R. Sato⁹, M. Schauer³⁴, V. Scherini⁴⁵, H. Schieler³⁶, M. Schimp³⁴,

D. Schmidt^{36,8}, O. Scholten^{78,c}, P. Schovánek²⁹, F.G. Schröder³⁶, S. Schröder³⁴, A. Schulz³⁵, J. Schumacher³⁸, S.J. Sciutto⁴, A. Segreto^{42,44}, R.C. Shellard¹⁴, G. Sigl³⁹, G. Silli^{8,36}, R. Šmída³⁶, G.R. Snow⁸⁹, P. Sommers⁸⁷, S. Sonntag⁴⁰, J. F. Soriano⁸³, R. Squartini⁹, D. Stanca⁷⁰, S. Stanić⁷³, J. Stasielak⁶⁶, P. Stassi³³, M. Stolpovskiy³³, F. Strafella^{53,45}, A. Streich³⁵, F. Suarez^{8,11}, M. Suarez Durán²⁷, T. Sudholz¹², T. Suomijärvi³¹, A.D. Supanitsky⁵, J. Šupík³⁰, J. Swain⁸⁶, Z. Szadkowski⁶⁸, A. Taboada³⁶, O.A. Taborda¹, V.M. Theodoro¹⁹, C. Timmermans^{79,77}, C.J. Todero Peixoto¹⁶, L. Tomankova³⁶, B. Tomé⁶⁹, G. Torralba Elipse⁷⁶, P. Travnicek²⁹, M. Trini⁷³, R. Ulrich³⁶, M. Unger³⁶, M. Urban³⁸, J.F. Valdés Galicia⁶⁵, I. Valiño⁷⁶, L. Valore^{57,47}, G. van Aar⁷⁷, P. van Bodegom¹², A.M. van den Berg⁷⁸, A. van Vliet⁷⁷, E. Varela⁶⁰, B. Vargas Cárdenas⁶⁵, R.A. Vázquez⁷⁶, D. Veberić³⁶, C. Ventura²⁵, I.D. Vergara Quispe⁴, V. Verzi⁴⁸, J. Vicha²⁹, L. Villaseñor⁶⁴, S. Vorobiov⁷³, H. Wahlberg⁴, O. Wainberg^{8,11}, D. Walz³⁸, A.A. Watson^a, M. Weber³⁷, A. Weindl³⁶, M. Wiedeński⁶⁸, L. Wiencke⁸², H. Wilczyński⁶⁶, T. Winchen³⁴, M. Wirtz³⁸, D. Wittkowski³⁴, B. Wundheiler⁸, L. Yang⁷³, A. Yushkov⁸, E. Zas⁷⁶, D. Zavrtanik^{73,74}, M. Zavrtanik^{74,73}, A. Zepeda⁶¹, B. Zimmermann³⁷, M. Ziolkowski⁴⁰, Z. Zong³¹, F. Zuccarello^{55,44}

— • —

- ¹ Centro Atómico Bariloche and Instituto Balseiro (CNEA-UNCuyo-CONICET), San Carlos de Bariloche, Argentina
- ² Centro de Investigaciones en Láseres y Aplicaciones, CITEDEF and CONICET, Villa Martelli, Argentina
- ³ Departamento de Física and Departamento de Ciencias de la Atmósfera y los Océanos, FCEyN, Universidad de Buenos Aires and CONICET, Buenos Aires, Argentina
- ⁴ IFLP, Universidad Nacional de La Plata and CONICET, La Plata, Argentina
- ⁵ Instituto de Astronomía y Física del Espacio (IAFE, CONICET-UBA), Buenos Aires, Argentina
- ⁶ Instituto de Física de Rosario (IFIR) – CONICET/U.N.R. and Facultad de Ciencias Bioquímicas y Farmacéuticas U.N.R., Rosario, Argentina
- ⁷ Instituto de Tecnologías en Detección y Astropartículas (CNEA, CONICET, UNSAM), and Universidad Tecnológica Nacional – Facultad Regional Mendoza (CONICET/CNEA), Mendoza, Argentina
- ⁸ Instituto de Tecnologías en Detección y Astropartículas (CNEA, CONICET, UNSAM), Buenos Aires, Argentina
- ⁹ Observatorio Pierre Auger, Malargüe, Argentina
- ¹⁰ Observatorio Pierre Auger and Comisión Nacional de Energía Atómica, Malargüe, Argentina
- ¹¹ Universidad Tecnológica Nacional – Facultad Regional Buenos Aires, Buenos Aires, Argentina
- ¹² University of Adelaide, Adelaide, S.A., Australia
- ¹³ Université Libre de Bruxelles (ULB), Brussels, Belgium
- ¹⁴ Centro Brasileiro de Pesquisas Físicas, Rio de Janeiro, RJ, Brazil
- ¹⁵ Centro Federal de Educação Tecnológica Celso Suckow da Fonseca, Nova Friburgo, Brazil
- ¹⁶ Universidade de São Paulo, Escola de Engenharia de Lorena, Lorena, SP, Brazil
- ¹⁷ Universidade de São Paulo, Instituto de Física de São Carlos, São Carlos, SP, Brazil
- ¹⁸ Universidade de São Paulo, Instituto de Física, São Paulo, SP, Brazil
- ¹⁹ Universidade Estadual de Campinas, IFGW, Campinas, SP, Brazil
- ²⁰ Universidade Estadual de Feira de Santana, Feira de Santana, Brazil
- ²¹ Universidade Federal de Pelotas, Pelotas, RS, Brazil
- ²² Universidade Federal do ABC, Santo André, SP, Brazil
- ²³ Universidade Federal do Paraná, Setor Palotina, Palotina, Brazil
- ²⁴ Universidade Federal do Rio de Janeiro, Instituto de Física, Rio de Janeiro, RJ, Brazil
- ²⁵ Universidade Federal do Rio de Janeiro (UFRJ), Observatório do Valongo, Rio de Janeiro, RJ, Brazil
- ²⁶ Universidade Federal Fluminense, EEIMVR, Volta Redonda, RJ, Brazil
- ²⁷ Universidad Industrial de Santander, Bucaramanga, Colombia

- ²⁸ Charles University, Faculty of Mathematics and Physics, Institute of Particle and Nuclear Physics, Prague, Czech Republic
- ²⁹ Institute of Physics of the Czech Academy of Sciences, Prague, Czech Republic
- ³⁰ Palacky University, RCPTM, Olomouc, Czech Republic
- ³¹ Institut de Physique Nucléaire d'Orsay (IPNO), Université Paris-Sud, Univ. Paris/Saclay, CNRS-IN2P3, Orsay, France
- ³² Laboratoire de Physique Nucléaire et de Hautes Energies (LPNHE), Universités Paris 6 et Paris 7, CNRS-IN2P3, Paris, France
- ³³ Laboratoire de Physique Subatomique et de Cosmologie (LPSC), Université Grenoble-Alpes, CNRS/IN2P3, Grenoble, France
- ³⁴ Bergische Universität Wuppertal, Department of Physics, Wuppertal, Germany
- ³⁵ Karlsruhe Institute of Technology, Institut für Experimentelle Kernphysik (IEKP), Karlsruhe, Germany
- ³⁶ Karlsruhe Institute of Technology, Institut für Kernphysik, Karlsruhe, Germany
- ³⁷ Karlsruhe Institute of Technology, Institut für Prozessdatenverarbeitung und Elektronik, Karlsruhe, Germany
- ³⁸ RWTH Aachen University, III. Physikalisches Institut A, Aachen, Germany
- ³⁹ Universität Hamburg, II. Institut für Theoretische Physik, Hamburg, Germany
- ⁴⁰ Universität Siegen, Fachbereich 7 Physik – Experimentelle Teilchenphysik, Siegen, Germany
- ⁴¹ Gran Sasso Science Institute (INFN), L'Aquila, Italy
- ⁴² INAF – Istituto di Astrofisica Spaziale e Fisica Cosmica di Palermo, Palermo, Italy
- ⁴³ INFN Laboratori Nazionali del Gran Sasso, Assergi (L'Aquila), Italy
- ⁴⁴ INFN, Sezione di Catania, Catania, Italy
- ⁴⁵ INFN, Sezione di Lecce, Lecce, Italy
- ⁴⁶ INFN, Sezione di Milano, Milano, Italy
- ⁴⁷ INFN, Sezione di Napoli, Napoli, Italy
- ⁴⁸ INFN, Sezione di Roma "Tor Vergata", Roma, Italy
- ⁴⁹ INFN, Sezione di Torino, Torino, Italy
- ⁵⁰ Osservatorio Astrofisico di Torino (INAF), Torino, Italy
- ⁵¹ Politecnico di Milano, Dipartimento di Scienze e Tecnologie Aerospaziali, Milano, Italy
- ⁵² Università del Salento, Dipartimento di Ingegneria, Lecce, Italy
- ⁵³ Università del Salento, Dipartimento di Matematica e Fisica "E. De Giorgi", Lecce, Italy
- ⁵⁴ Università dell'Aquila, Dipartimento di Scienze Fisiche e Chimiche, L'Aquila, Italy
- ⁵⁵ Università di Catania, Dipartimento di Fisica e Astronomia, Catania, Italy
- ⁵⁶ Università di Milano, Dipartimento di Fisica, Milano, Italy
- ⁵⁷ Università di Napoli "Federico II", Dipartimento di Fisica "Ettore Pancini", Napoli, Italy
- ⁵⁸ Università di Roma "Tor Vergata", Dipartimento di Fisica, Roma, Italy
- ⁵⁹ Università Torino, Dipartimento di Fisica, Torino, Italy
- ⁶⁰ Benemérita Universidad Autónoma de Puebla, Puebla, México
- ⁶¹ Centro de Investigación y de Estudios Avanzados del IPN (CINVESTAV), México, D.F., México
- ⁶² Unidad Profesional Interdisciplinaria en Ingeniería y Tecnologías Avanzadas del Instituto Politécnico Nacional (UPIITA-IPN), México, D.F., México
- ⁶³ Universidad Autónoma de Chiapas, Tuxtla Gutiérrez, Chiapas, México
- ⁶⁴ Universidad Michoacana de San Nicolás de Hidalgo, Morelia, Michoacán, México
- ⁶⁵ Universidad Nacional Autónoma de México, México, D.F., México
- ⁶⁶ Institute of Nuclear Physics PAN, Krakow, Poland
- ⁶⁷ University of Łódź, Faculty of Astrophysics, Łódź, Poland
- ⁶⁸ University of Łódź, Faculty of High-Energy Astrophysics, Łódź, Poland
- ⁶⁹ Laboratório de Instrumentação e Física Experimental de Partículas – LIP and Instituto Superior Técnico – IST, Universidade de Lisboa – UL, Lisboa, Portugal
- ⁷⁰ "Horia Hulubei" National Institute for Physics and Nuclear Engineering, Bucharest-Magurele, Romania
- ⁷¹ Institute of Space Science, Bucharest-Magurele, Romania
- ⁷² University Politehnica of Bucharest, Bucharest, Romania

- ⁷³ Center for Astrophysics and Cosmology (CAC), University of Nova Gorica, Nova Gorica, Slovenia
- ⁷⁴ Experimental Particle Physics Department, J. Stefan Institute, Ljubljana, Slovenia
- ⁷⁵ Universidad de Granada and C.A.F.P.E., Granada, Spain
- ⁷⁶ Universidad de Santiago de Compostela, Santiago de Compostela, Spain
- ⁷⁷ IMAPP, Radboud University Nijmegen, Nijmegen, The Netherlands
- ⁷⁸ KVI – Center for Advanced Radiation Technology, University of Groningen, Groningen, The Netherlands
- ⁷⁹ Nationaal Instituut voor Kernfysica en Hoge Energie Fysica (NIKHEF), Science Park, Amsterdam, The Netherlands
- ⁸⁰ Stichting Astronomisch Onderzoek in Nederland (ASTRON), Dwingeloo, The Netherlands
- ⁸¹ Case Western Reserve University, Cleveland, OH, USA
- ⁸² Colorado School of Mines, Golden, CO, USA
- ⁸³ Department of Physics and Astronomy, Lehman College, City University of New York, Bronx, NY, USA
- ⁸⁴ Michigan Technological University, Houghton, MI, USA
- ⁸⁵ New York University, New York, NY, USA
- ⁸⁶ Northeastern University, Boston, MA, USA
- ⁸⁷ Pennsylvania State University, University Park, PA, USA
- ⁸⁸ University of Chicago, Enrico Fermi Institute, Chicago, IL, USA
- ⁸⁹ University of Nebraska, Lincoln, NE, USA
-
- ^a School of Physics and Astronomy, University of Leeds, Leeds, United Kingdom
- ^b Max-Planck-Institut für Radioastronomie, Bonn, Germany
- ^c also at Vrije Universiteit Brussels, Brussels, Belgium
- ^d SUBATECH, École des Mines de Nantes, CNRS-IN2P3, Université de Nantes, France
- ^e Fermi National Accelerator Laboratory, USA
- ^f Colorado State University, Fort Collins, CO
- ^g now at Deutsches Elektronen-Synchrotron (DESY), Zeuthen, Germany
- [†] Deceased

Acknowledgments of the Telescope Array Collaboration

The Telescope Array experiment is supported by the Japan Society for the Promotion of Science through Grants-in-Aid for Scientific Research on Specially Promoted Research (21000002) “Extreme Phenomena in the Universe Explored by Highest Energy Cosmic Rays” and for Scientific Research (19104006), and the Inter-University Research Program of the Institute for Cosmic Ray Research; by the U.S. National Science Foundation awards PHY-0601915, PHY-1404495, PHY-1404502, and PHY1607727; by the National Research Foundation of Korea (2015R1A2A1A-01006870, 2015R1A2A1A15055344, 2016R1A5A1013277, 2007-0093860, 2016R1A2B4014967); by the Russian Academy of Sciences, RFBR grant 16-02-00962a (INR), IISN project No. 4.4502.13, and Belgian Science Policy under IUAP VII/37 (ULB). The foundations of Dr. Ezekiel R. and Edna Wattis Dumke, Willard L. Eccles, and George S. and Dolores Doré Eccles all helped with generous donations. The State of Utah supported the project through its Economic Development Board, and the University of Utah through the Office of the Vice President for Research. The experimental site became available through the cooperation of the Utah School and Institutional Trust Lands Administration (SITLA), U.S. Bureau of Land Management (BLM), and the U.S. Air Force. We appreciate the assistance of the State of Utah and Fillmore offices of the BLM in crafting the Plan of Development for the site. Patrick Shea assisted the collaboration with valuable advice on a variety of topics. The people and the officials of Millard County, Utah have been a source of steadfast and warm support for our work which we greatly appreciate. We are indebted to the Millard County Road Department for their efforts to maintain and clear the roads which get us to our sites. We gratefully acknowledge the contribution from the technical staffs of our home institutions. An allocation of computer time from the Center for High Performance Computing at the University of Utah is gratefully acknowledged.

Acknowledgments of the Pierre Auger Collaboration

The successful installation, commissioning, and operation of the Pierre Auger Observatory would not have been possible without the strong commitment and effort from the technical and administrative staff in Malargüe. We are very grateful to the following agencies and organizations for financial support:

Argentina – Comisión Nacional de Energía Atómica; Agencia Nacional de Promoción Científica y Tecnológica (ANPCyT); Consejo Nacional de Investigaciones Científicas y Técnicas (CONICET); Gobierno de la Provincia de Mendoza; Municipalidad de Malargüe; NDM Holdings and Valle Las Leñas; in gratitude for their continuing cooperation over land access; Australia – the Australian Research Council; Brazil – Conselho Nacional de Desenvolvimento Científico e Tecnológico (CNPq); Financiadora de Estudos e Projetos (FINEP); Fundação de Amparo à Pesquisa do Estado de Rio de Janeiro (FAPERJ); São Paulo Research Foundation (FAPESP) Grants No. 2010/07359-6 and No. 1999/05404-3; Ministério de Ciência e Tecnologia (MCT); Czech Republic – Grant No. MSMT CR LG15014, LO1305, LM2015038 and CZ.02.1.01/0.0/0.0/16_013/0001402; France – Centre de Calcul IN2P3/CNRS; Centre National de la Recherche Scientifique (CNRS); Conseil Régional Ile-de-France; Département Physique Nucléaire et Corpusculaire (PNC-IN2P3/CNRS); Département Sciences de l’Univers (SDU-INSU/CNRS); Institut Lagrange de Paris (ILP) Grant No. LABEX ANR-10-LABX-63 within the Investissements d’Avenir Programme Grant No. ANR-11-IDEX-0004-02; Germany – Bundesministerium für Bildung und Forschung (BMBF); Deutsche Forschungsgemeinschaft (DFG); Finanzministerium Baden-Württemberg; Helmholtz Alliance for Astroparticle Physics (HAP); Helmholtz-Gemeinschaft Deutscher Forschungszentren (HGF); Ministerium für Innovation, Wissenschaft und Forschung des Landes Nordrhein-Westfalen; Ministerium für Wissenschaft, Forschung und Kunst des Landes Baden-Württemberg; Italy – Istituto Nazionale di Fisica Nucleare (INFN); Istituto Nazionale di Astrofisica (INAF); Ministero dell’Istruzione, dell’Università e della Ricerca (MIUR); CETEMPS Center of Excellence; Ministero degli Affari Esteri (MAE); Mexico – Consejo Nacional de Ciencia y Tecnología (CONA-

CYT) No. 167733; Universidad Nacional Autónoma de México (UNAM); PAPIIT DGAPA-UNAM; The Netherlands – Ministerie van Onderwijs, Cultuur en Wetenschap; Nederlandse Organisatie voor Wetenschappelijk Onderzoek (NWO); Stichting voor Fundamenteel Onderzoek der Materie (FOM); Poland – National Centre for Research and Development, Grants No. ERA-NET-ASPERA/01/11 and No. ERA-NET-ASPERA/02/11; National Science Centre, Grants No. 2013/08/M/ST9/00322, No. 2013/08/M/ST9/00728 and No. HARMONIA 5–2013/10/M/ST9/00062, UMO-2016/22/M/ST9/00198; Portugal – Portuguese national funds and FEDER funds within Programa Operacional Factores de Competitividade through Fundação para a Ciência e a Tecnologia (COMPETE); Romania – Romanian Authority for Scientific Research ANCS; CNDI-UEFISCDI partnership projects Grants No. 20/2012 and No. 194/2012 and PN 16 42 01 02; Slovenia – Slovenian Research Agency; Spain – Comunidad de Madrid; Fondo Europeo de Desarrollo Regional (FEDER) funds; Ministerio de Economía y Competitividad; Xunta de Galicia; European Community 7th Framework Program Grant No. FP7-PEOPLE-2012-IEF-328826; USA – Department of Energy, Contracts No. DE-AC02-07CH11359, No. DE-FR02-04ER41300, No. DE-FG02-99ER41107 and No. DE-SC0011689; National Science Foundation, Grant No. 0450696; The Grainger Foundation; Marie Curie-IRSES/EPLANET; European Particle Physics Latin American Network; European Union 7th Framework Program, Grant No. PIRSES-2009-GA-246806; European Union's Horizon 2020 research and innovation programme (Grant No. 646623); and UNESCO.

Contributions

- 1 Sean Quinn: *Auger at the Telescope Array: toward a direct cross-calibration of surface-detector stations* 10
- 2 Dmitri Ivanov: *Report of the Telescope Array – Pierre Auger Observatory Working Group on Energy Spectrum* 18
- 3 Vitor de Souza: *Testing the agreement between the X_{\max} distributions measured by the Pierre Auger and Telescope Array Observatories* 25



Auger at the Telescope Array: toward a direct cross-calibration of surface-detector stations

**S. Quinn^{*1} for the Pierre Auger Collaboration^a and Telescope Array Collaboration^b;
S. Colognes², B. Courty², B. Genolini³, L. Guglielmi², P. Lebrun⁴, M. Marton⁵,
E. Raully³, T. Trung³, O. Wolf⁶**

¹*Dept. of Physics, Case Western Reserve Univ., Cleveland, Ohio, USA*

²*Laboratoire Astroparticules et Cosmologie (APC), Univ. Paris 7, CNRS-IN2P3, Paris, France*

³*Institut de Physique Nucléaire d'Orsay (IPNO), Univ. Paris 11, CNRS-IN2P3, Orsay, France*

⁴*Fermilab, Batavia IL, USA*

⁵*Laboratoire de Physique Subatomique et de Cosmologie (LPSC), Univ. Joseph Fourier, INPG, CNRS-IN2P3, Grenoble, France*

⁶*Physics Department, Colorado School of Mines, Golden CO, USA*

^a*Observatorio Pierre Auger, Av. San Martín Norte 304, 5613 Malargüe, Argentina*

E-mail: auger_spokespersons@fnal.gov

Full author list: http://auger.org/archive/authors_icrc_2017.html

^b*Telescope Array Project, 201 James Fletcher Bldg., 115 S. 1400 East, Salt Lake City, UT 84112-0830, USA*

E-mail: ta-icrc@cosmic.utah.edu

Full author list: <http://telescopearray.org/index.php/research/collaborators>

Since 2007 the Telescope Array Project (TA) and Pierre Auger Observatory (Auger) have collected extensive data sets spanning several orders of magnitude of the cosmic-ray spectrum. In both experiments the majority of data is generated from the surface-detector (SD) array as a result of its very high duty cycle. These data are then calibrated for energy with fluorescence detectors using a hybrid approach. The TA and Auger experiments use different SD station designs, giving them different sensitivities to extensive air-shower components. We seek to understand and cross-validate these complementary detectors on a hardware level. In this paper we present an update on the progress of this in-situ cross-calibration program. Presently two Auger water-Cherenkov detectors and two TA scintillator stations are co-located at the TA central laser facility (CLF). We review the hardware enabling the readout of these detectors for high-energy events. Additionally, we show expanded calibration data sets of minimum-ionizing particle (MIP) versus vertical-equivalent muon (VEM) responses, along with preliminary results for the Auger doublet. A sample event reconstruction displaying observed Auger and TA signals is also presented.

*35th International Cosmic Ray Conference — ICRC2017
10–20 July, 2017
Bexco, Busan, Korea*

^{*}Speaker.

1. Introduction

The Pierre Auger Observatory is a hybrid cosmic-ray (CR) experiment located in Mendoza, Argentina, which detects extensive air showers (EAS) using four fluorescence-telescope detectors and 1660 surface-detector (SD) stations [1]. Fluorescence observations provide high-quality data of shower energy as well as depth of maximum shower development, important for composition studies, but have a limited duty cycle. The subset of hybrid events passing stringent quality cuts is used to calibrate “SD only” events which account for the majority of reconstructed EAS data.

The Telescope Array Project is also a hybrid CR observatory located in central Utah, USA [2]. In addition to its three fluorescence-telescope detector stations, TA operates 507 SD stations, with ~ 400 more detectors being introduced over the next few years to quadruple the detection area [3]. Both experiments utilize SD stations with self-contained electronics, communications, and solar power systems. The detection medium in Auger is used to count air-shower muons but is also sensitive to the electromagnetic shower component, while TA detectors count ionizing particles indiscriminately.

The Auger SD station is a water-Cherenkov detector (WCD). Relativistic leptons and high-energy photons generate signals via Cherenkov radiation and pair production, respectively, which are collected by photomultiplier tubes (PMTs). The Telescope Array SD station uses plastic scintillator panels. Fluorescent scintillation light is collected by wavelength-shifting fibers and guided to PMTs in a dual layer setup.

To improve understanding of the energy spectrum and origin of ultrahigh-energy cosmic rays (UHECRs), the TA and Auger Collaborations have performed analyses of a joint data set [4, 5]. These studies benefit from larger statistics and full sky coverage. A recent analysis [5] concluded that UHECR composition results of both experiments agree within systematic uncertainties. The energy spectra also agree within systematic errors up to the ankle, but diverge toward the highest energies ($E \gtrsim 50$ EeV) near the Greisen, Zatsepin, Kuz'min (GZK) cutoff [6, 7]. The source of this discrepancy remains to be fully explained, but possibilities might include: the result of experimental effects or different astrophysics scenarios in the northern and southern skies. We are investigating the possibility of energy-dependent experimental effects using a direct comparison of surface-detection methods through a two-phase joint cross-calibration program. Phase I, where data for station-level responses to the same air shower is compared, has been underway for roughly 8 months. We review results from earlier work [8, 9], provide an overview of hardware deployed and prototypes in development, and present an updated cross calibration curve along with an example shower reconstruction.

2. Detectors in the field

For phase I we are currently collecting data from: one Auger south (AS) WCD, one prototype Auger north (AN) WCD and two TA stations (see Figure 1). The AN and AS doublet is formed to study the response between the conventional AS station (used at the Pierre Auger Observatory) and prototype AN station.

The AS and AN detectors use a 3.6 m diameter, 1.2 m high, reflectively lined (Tyvek ®) tank filled with 12,000 L of purified water. In AS three symmetrically distributed PMTs, each 1.2 m

from the central axis [1], are used. Low-gain (AC coupled anode) and high-gain (8th dynode) channels for each PMT are input to the electronics and digitized by 10-bit 40 MHz semi-flash ADCs. These traces are analyzed and time-stamped (GPS synchronized clock) by a programmable logic device running triggering firmware. A data-acquisition (DAQ) system running on a single board computer (SBC) (see section 3.1) evaluates the timestamps of station-level (T2) events. Coincident time-stamps in a certain geometry surrounding the central laser facility (CLF) generate a physics trigger—the SBC requests the stations to transfer ADC traces for the event. Online calibration data from the previous minute for AS, and the previous 14 minutes for AN, are also retrieved to convert each ADC waveform to an integrated vertical muon-equivalent signal (VEM).

The AN station uses a single, central, downward facing 9" PMT. The electronics are similar to AS, but use fewer components since only one PMT is digitized. The key difference is a new 10-bit 100-MHz flash ADC (FADC) which processes four channels for increased dynamic range as well as a new Linux based operating system (Debian) which includes many convenient applications. The anode signal is split into $0.1\times$, $1\times$, and $30\times$ channels. Instead of the 8th dynode, the 5th stage is used to achieve a larger overall dynamic range.

The TA station uses two layers of polyvinyl toluene scintillators 3 m^2 in area and 1.2 cm thick. In each layer, light is guided through 104 wavelength shifting fibers to a 30 mm PMT. The anode is digitized by 12-bit 50-MHz FADCs which are processed by triggers implemented on field-programmable gate arrays (FPGA) and transmitted as station-level (L1) events. A hierarchical triggering system is implemented based on minimum-ionizing particles (MIP). Station-level events are communicated wirelessly to a central acquisition computer. Physics triggers are similar to those in the Auger array, requiring a coincidence of geometrical and temporal station-level events.

The four detectors are co-located at the CLF site. The Auger doublet is located in the northeast corner, one TA station is in the northwest and the other in the southwest corner. The maximum separation between stations is $\approx 44\text{ m}$ from the Auger doublet to the southwest TA station.



Figure 1: Photo of hardware deployed at the TA CLF site. Custom cabling was setup along guy wires from stations to the CLF for data acquisition. North is to the right of the page.

3. DAQ setup

3.1 High-level description

To retrieve data from the Auger stations, which are designed to operate wirelessly, we modified the electronics to communicate over a physical wire connected to a SBC housed inside the CLF. An

external trigger is required to read out the Auger doublet for low-energy events which is provided by a primitive threshold-comparator circuit attached to a bare (without electronics) TA SD station: this is known as the “local trigger”. For a direct comparison between Auger and TA waveforms, a second fully functional TA station was installed in the southwest corner and is able to send data for physics events (higher energy showers) using the standard TA radio protocol.

3.2 TA global (physics) trigger

During March 2016 a TA SD electronics kit was brought online inside the CLF container. It uses a parabolic radio antenna to listen for physics triggers sent to the TA SD array. The firmware was modified to relay time-stamp information for shower candidates observed by the TA DAQ computer and is forwarded over a RS-232 serial connection to the SBC inside the CLF.

The southwest “global” TA station (DET2421 in Figure 1) uses standard TA electronics and operates in normal TA acquisition mode. The L1 time stamps from this detector are ignored by the TA DAQ computer—hence this station does *not* participate with adjacent stations to contribute toward the physics/array trigger. However, when an event is observed it transmits data normally. The relevant traces for this project are only collected when a core lands in a constrained area of CLF neighboring stations. Auger traces are also retrieved for the global trigger timestamp, so a direct comparison of station waveforms is possible. With the appropriate conversion between MIP and VEM, it is also possible to insert Auger data into a lateral distribution function (LDF) to optionally perform a dual detector reconstruction.

3.3 CLF vicinity “local” trigger

The northwest TA station, installed August 2016, is used to investigate showers of low and intermediate-energy with cores close to the CLF. Currently it only operates as an external trigger for the Auger doublet until a way to collect the TA waveforms over a wired connection is devised. It is roughly 32 m from the doublet. The PMTs are operated nominally at -1.2 kV, and when the anode output of both simultaneously cross a threshold set at < -92 mV the circuit transmits a logic pulse over a RG58 cable to a development FPGA board (MicroZed) running time-tagging firmware referenced to GPS time. The signal is time-stamped and sent over a serial connection to the Auger SBC (Raspberry Pi 2 Model B). This station is operated at a base rate of $\approx 3\text{--}15$ Hz.

3.4 Trigger decision hardware and software

Custom interconnects and cabling bring AN CANbus and AS RS-232 serial data into the CLF in place of radios. A radio-protocol emulation program on the SBC is used to decode AS data and send control or read out commands to the AS station, while similar software handles AN communication. These packages provide real-time station-level event lists (T2 triggers). These lists, combined with another program which parses the CLF local and global triggers, are analyzed for coincidences. A read out request (T3 trigger) is sent if the time difference between the Auger doublet event and global event is $< 100\ \mu\text{s}$, or if the local trigger and Auger doublet difference is $< 20\ \mu\text{s}$. A high-level diagram of the setup is displayed in Figure 2. Auger north can optionally be configured to save its data to a local disk.

Events are archived by day (UTC) and uploaded to remote servers where data decompression and analysis are performed using code written for this project. Monitoring and detector performance information is updated daily.

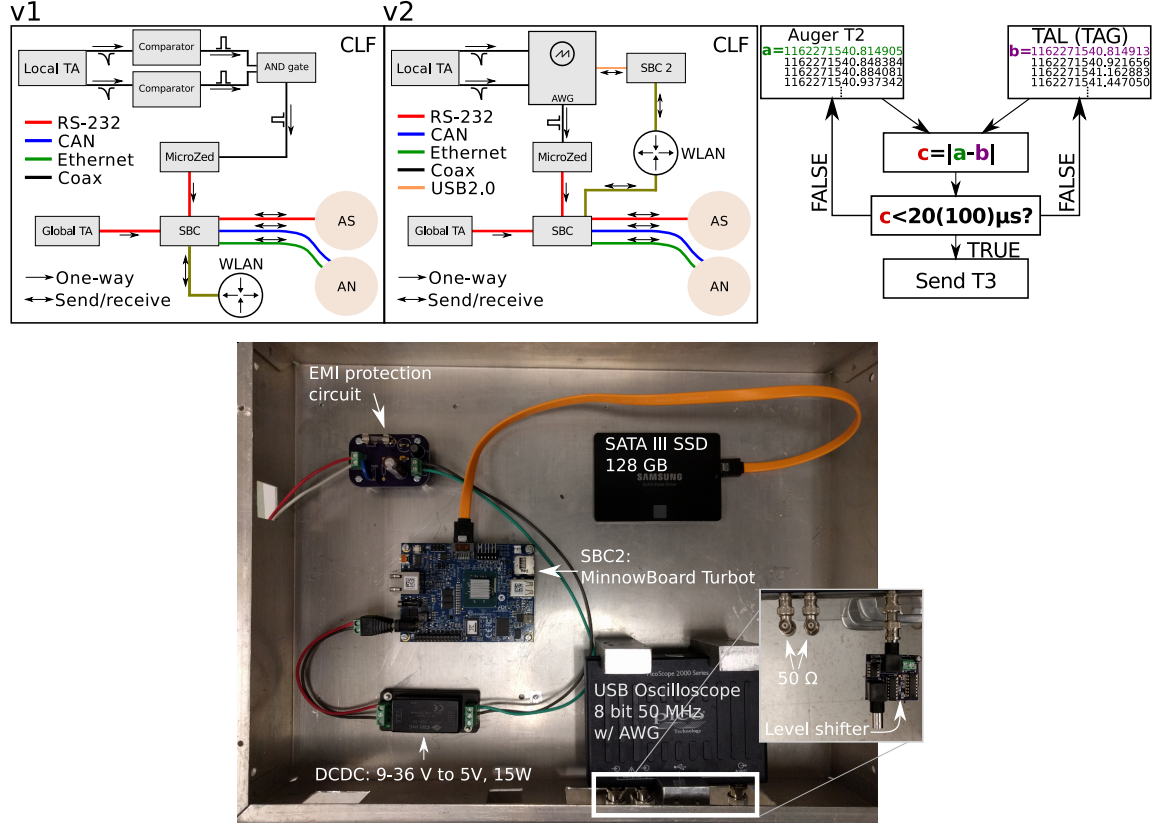


Figure 2: *Top left:* block diagram of current local trigger hardware deployed at the CLF site (see text for details). *Top middle:* future local trigger setup under development. *Top right:* trigger-condition flow chart showing the “do while” loop to compare example local time stamps. Items in parentheses refer to the global trigger. *Bottom:* photo of the future prototype local trigger hardware to be installed in the field.

3.4.1 Prototype advanced local trigger design

The current local trigger design uses a simple threshold comparator circuit which measures the peak amplitude of PMT waveforms. This results in a bias favoring inclined “old” showers dominated by muons, compared to vertical “young” showers where the signal is spread out in time and contains a larger fraction of electromagnetic components. Also, the current setup doesn’t provide any information about the waveform morphology initiating the trigger.

To address this limitation we have developed a new prototype local trigger system which uses a Pico Technology 2206B USB oscilloscope connected to a Minnowboard Turbot SBC. Using the Pico software, we can remotely configure programmable triggers to fire on temporal features in addition to threshold levels. This setup offers a closer approximation to Auger and TA station level triggers in lieu of TA electronics for the local detector. The new SBC is equipped with a hard drive so calibration data and event waveforms can be stored. The associated time stamp is relayed from

the SBC inside the CLF over the local network. The prototype will be a drop-in replacement for the current circuit—a diagram and photo of the design is shown in Figure 2.

4. Analysis & Results

4.1 Auger north and south comparison

The Auger doublet is used to study the performance of AN and AS observations for the same EAS. From November 2016 through May 2017 we have recorded 1635 coincidences generated by the external local trigger. We show logarithmized data in Figure 3, along with a fit. No quality cuts or VEM thresholds have been applied. We find a least squares best fit power law of $S_{AS} = 1.18(S_{AN})^{0.92}$. The ideal expectation is $S_{AS} = S_{AN}$, however it must be stressed our calibration source is low energy showers with small cores and potentially highly variable particle densities. It is not possible to do any post selection with our current setup—Poissonian fluctuations are included. We will continue to investigate this correlation. To test the responses using a more constrained input, we look at signal correlations for global events where both stations have data. For this comparison we find a best fit powerlaw of $S_{AS} = 0.76(S_{AN})^{1.06}$.

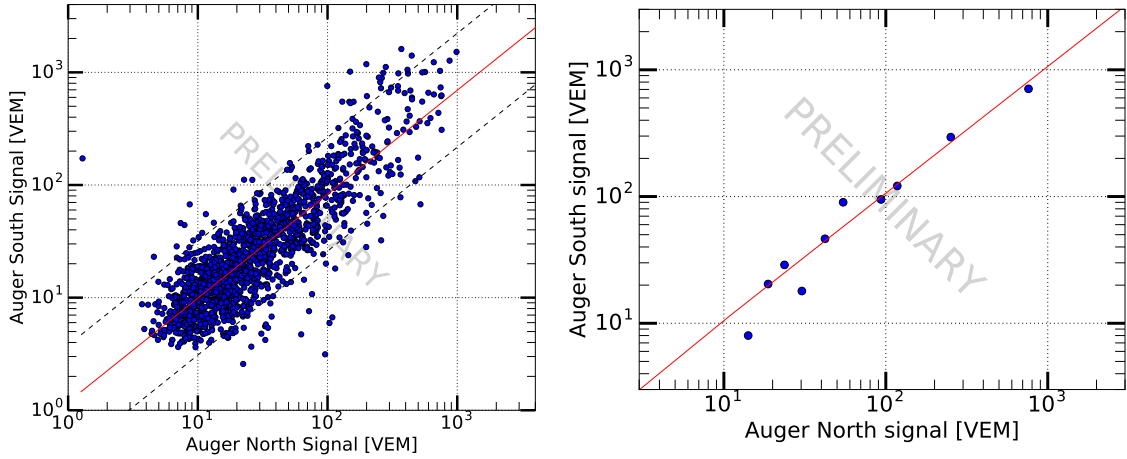


Figure 3: *Left:* Auger south and Auger north signal pairs for local events. Solid red line is the least squares fit and dashed black lines are the 95% prediction interval. *Right:* Auger south and Auger north signal pairs for global events only. Best fit line is solid red.

4.2 Global event reconstruction and trace comparison

We have collected 54 global coincidences between the AS and neighboring TA stations up to May 2017. In Figure 4 we show FADC waveforms and core position for a single event within 2 km from the CLF. This is one of the 8 events in the data set which passes standard TA SD quality cuts outlined in [10]. From a TA reconstruction we find the following observables: $E = 4.58$ EeV, $(\theta, \varphi) = (38.28, 216.69)^\circ$ and $r = 0.82$ km, where E , (θ, φ) and r are primary energy, zenith & azimuth angles and core distance, respectively. Using the standard calibration techniques, we find average integrated signals of 36.58 MIP and 56.50 VEM. In addition to a comparison of integrated signals, we can also compare waveform shapes, but we reserve this for a future study.

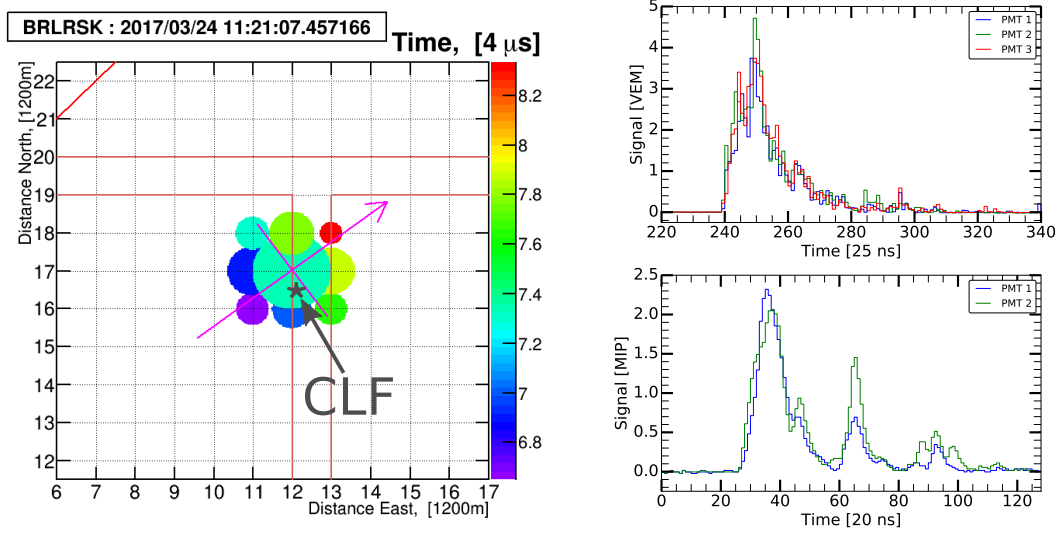


Figure 4: *Left:* position and timing information for a global event also seen by TA and Auger detectors co-located at CLF. *Top right:* Auger south high gain waveforms. *Bottom right:* DET2421 waveforms.

4.3 MIP vs. VEM cross-calibration curve and simulations

The global event data can be used to form a cross calibration curve for MIP and VEM signals, see Figure 5. With more statistics this curve can be used to study detector responses to the same shower, and, further, how any potential difference in detector sensitivity depends on air-shower parameters. For phase II this curve can be used to translate between MIP and VEM signals.

We present an initial result for such a study using simulations in the Auger Offline framework [1] with newly implemented scintillator detectors [11] on top of a WCD. To start, an ad-hoc Monte Carlo (MC) shower population was generated with the following parameter space: $E = 3.98 \text{ EeV}$, $\theta = \{0, 12, 25, 36, 45, 53\}^\circ$, $r = 600 \text{ m}$. The Auger scintillator has an area of 4 m^2 while a TA SD is 3 m^2 : the integrated TA MIP values will roughly scale as 0.75 of the Auger scintillator MIP values. We show these simulations and a recently updated MIP vs. VEM plot in Figure 5. For the current data set, DET2421 and Auger signal responses and by extension TA reconstruction parameters, appear to be consistent with these simulations. More detailed event-by-event shower and reconstruction simulations are underway.

5. Conclusion

In this work we have highlighted progress made since the publication of [8, 9]. Initial results of the Auger doublet correlation for a highly variable input population appears reasonable. The doublet data for select global events is more tightly correlated. We presented a reconstruction with corresponding waveforms for a sample event. An updated MIP-VEM cross-calibration curve was shown for all raw data as well as events which pass a standard quality cut. These data were compared to MC simulations using a prototype Auger upgrade detector for a variety of shower parameters—while preliminary, the data mostly agree with these simulations. Initial designs to improve the local trigger system were proposed, and phase II was briefly motivated.

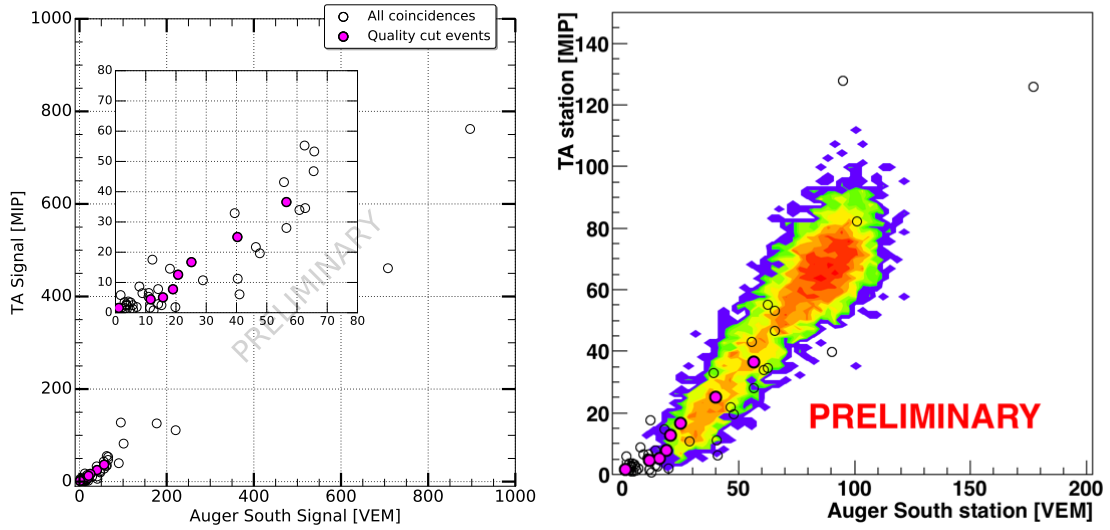


Figure 5: *Left:* cross-calibration curve for most recent data set. Open black circles include all global trigger data while filled magenta circles are events that pass quality cuts [10]. Inset plot is zoomed in area of signals with < 80 VEM/MIP. *Right:* Similar to left inset, but with MC simulation contours overlaid.

Acknowledgements

This project was supported in part by JSPS Grant-in-Aid for Scientific Research (A) 25247035.

References

- [1] The Pierre Auger Collaboration, [Nucl. Instr. Meth. Phys. Res. A **798**, 172 \(2015\)](#)
- [2] The Telescope Array Collaboration, [Nucl. Instr. Meth. Phys. Res. A **689**, 87 \(2012\)](#)
- [3] H. Sagawa for the Telescope Array Collaboration, Proc. of the 34th Int. Cosmic Ray Conf., The Hague, The Netherlands, [PoS\(ICRC2015\)657 \(2015\)](#)
- [4] O. Deligny for the Pierre Auger and Telescope Array Collaborations, Proc. of the 34th Int. Cosmic Ray Conf., The Hague, The Netherlands, [PoS\(ICRC2015\)395 \(2015\)](#)
- [5] M. Unger for the Pierre Auger and Telescope Array Collaborations, Proc. of the 34th Int. Cosmic Ray Conf., The Hague, The Netherlands, [PoS\(ICRC2015\)307 \(2015\)](#)
- [6] K. Greisen, [Phys. Rev. Lett. **16**, 748 \(1966\)](#)
- [7] G. T. Zatsepin, V. A. Kuz'min, [JETPL **4**, 78Z \(1966\)](#)
- [8] R. Takeishi for the Pierre Auger and Telescope Array Collaborations, Proc. of the 34th Int. Cosmic Ray Conf., The Hague, The Netherlands, [PoS\(ICRC2015\)393 \(2015\)](#)
- [9] S. Quinn for the Pierre Auger and Telescope Array Collaborations, Proc. of Int. Symposium for UHECRs, Kyoto, Japan. Submitted for publication (2017)
- [10] The Telescope Array Collaboration, [ApJ **768**, L1 \(2013\)](#)
- [11] The Pierre Auger Collaboration, The Pierre Auger Observatory Upgrade - Preliminary Design Report, [arXiv:1604.03637 \(2016\)](#)



Report of the Telescope Array – Pierre Auger Observatory Working Group on Energy Spectrum

**Dmitri Ivanov^{*a}, for the Pierre Auger Collaboration^b and the Telescope Array
Collaboration^c**

^a*University of Utah, Department of Physics & Astronomy and High Energy Astrophysics Institute,
Salt Lake City, Utah, USA*

E-mail: dmiivanov@gmail.com

^b*Observatorio Pierre Auger, Av. San Martín Norte 304, 5613 Malargüe, Argentina*

E-mail: auger_spokespersons@fnal.gov

Full author list: http://www.auger.org/archive/authors_icrc_2017.html

^c*Telescope Array Project, 201 James Fletcher Bldg, 115 S. 1400 East, Salt Lake City, UT
84112-0830, USA*

E-mail: ta-icrc@cosmic.utah.edu

Full author list: <http://www.telescopearray.org/index.php/research/collaborators>

The Telescope Array and Pierre Auger Collaborations have formed a working group to examine the similarities and differences in their measurements of the spectrum of ultra-high energy cosmic rays. The method chosen is for each experiment to measure the spectrum in the declination band of $-15.7^\circ < \delta < 24.8^\circ$, where both experiments have sensitivity. A second step chosen is to correct for the weighting in declination over each experiment's range of sensitivity in the common band of declinations.

*35th International Cosmic Ray Conference — ICRC217
10–20 July, 2017
Bexco, Busan, Korea*

^{*}Speaker.

1. Introduction

The energy spectrum of ultra-high energy cosmic rays (UHECRs) is important for understanding their origin and mechanisms of acceleration and propagation. The UHECR energy spectrum working group (WG) was first proposed at the UHECR-2010 conference in Nagoya, Japan, and a detailed comparison of Pierre Auger Observatory, Telescope Array, Yakutsk, HiRes, and AGASA spectra was presented at the UHECR-2012 conference at CERN [1]. It was concluded that the features seen by all five experiments were consistent among each other after taking into account the differences of their energy scales. For example, at that time, a relative shift of 20% in energies between the TA and Auger would bring the two results into agreement. It was then understood that the future studies of UHECRs have to rely heavily on the measurements of the Auger Observatory and the Telescope Array, the two largest cosmic ray detectors which use a hybrid design that allows calibrating the energy scale of the surface detector (SD) to the fluorescence detector (FD) on an event by event basis. A fluorescence detector gives a nearly calorimetric estimate of the UHECR energy.

Subsequent results of the WG were reported at the UHECR 2014 conference in Springdale, Utah (USA) [2]. The discussion was focused on the TA and Auger. It was then established that the use of different fluorescence yield models and invisible energy corrections by the two experiments were the largest contributions to the relative energy scale shift, which at that time was estimated to be 16%. The conclusion was that the Auger and TA spectra were in a good agreement in the region around the *ankle*, while a significant difference became apparent at the highest energies, in the region of the suppression.

In this work, we update the recent results of the WG presented at the UHECR conference held in Kyoto (Japan), in Fall 2016 [3], compare the measurements of the UHECR spectrum by Auger and TA, and discuss their differences.

2. TA and Auger spectrum

Auger and TA are the largest cosmic ray detectors in the Southern and the Northern hemispheres, respectively. Auger [4] is located in the province of Mendoza (Argentina), near the town of Malargüe. Auger consists of an SD array of 1,660 water-Cherenkov detectors, arranged on a 1.5 km spaced triangular grid, with 5 FD stations overlooking the array. The Auger SD effectively covers a 3,000 km² area on the ground with an altitude of approximately 1,400 m above sea level. The TA experiment is located in Millard County, Utah (USA), in the desert near the town of Delta. The TA SD [5] consists of 507 plastic scintillation counters arranged on a square grid of 1.2 km spacing, and it is overlooked by 3 FDs [6, 7]. TA SD covers 700 km² on the ground. The altitude of the TA SD is also approximately 1,400 m above sea level. In both TA and Auger, the UHECR energy spectrum is measured with best statistics by the SDs.

Auger uses two methods to reconstruct SD events: one for events with zenith angles below 60°, called *vertical* events, and another for events with zenith angles between 60° and 80°, called *inclined* events. Minimum energies are adjusted for each reconstruction type separately, so that the analyses are fully efficient. The minimum energies are 3×10^{18} eV and 4×10^{18} eV for *vertical* and *inclined* events, respectively. In TA, the energy spectrum measurement that begins at $10^{18.2}$ eV

uses events with zenith angles below 45° (seen in Figure 1), while the measurement that starts at 10^{19} eV uses events up to 55° in zenith angle (seen in Figures 3, and 5). The Auger and TA SD energy spectra are shown in the left panel of Figure 1, multiplied by energy cubed to emphasize the changes in the power law. Both Auger and TA clearly see the ankle and the suppression. Evidently, there is an overall energy scale difference between the two measurements, as well as (possibly) energy-dependent differences: if fitted to a broken power law shape, the Auger second break point occurs at $10^{19.62 \pm 0.02}$ eV, while the corresponding break in TA is seen at $10^{19.78 \pm 0.06}$ eV, a factor of 1.4 ± 0.2 higher.

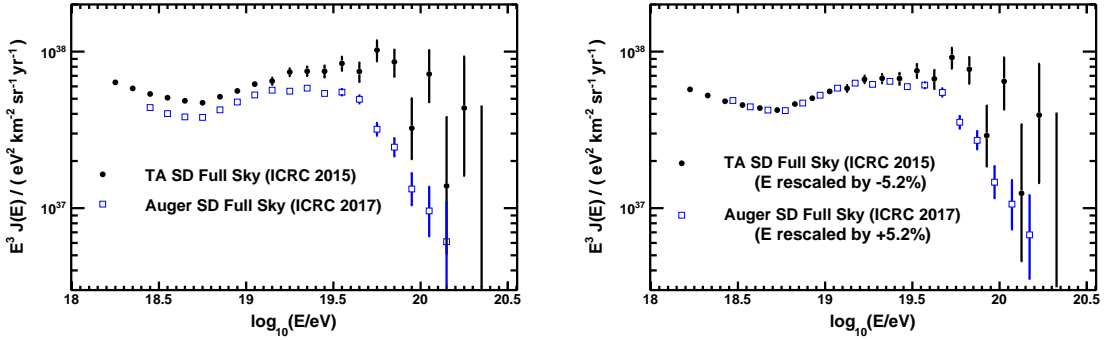


Figure 1: Energy spectrum measurements by the Auger [8] and TA [9] surface detectors. Left: Using energy scales of Auger and TA. Right: TA energy scale is reduced by 5.2% while Auger energy scale is increased by 5.2%.

As pointed out in Section 1, although the TA and Auger techniques of reconstructing SD event energies are very similar, there do exist differences in their respective instruments and the methods of how the final primary energies are assigned. The systematic uncertainty in the overall energy scale is 14% for Auger and 21% for TA, while the uncertainties due to the exposure and the unfolding of the effects of the resolution are subdominant. As the right panel of the Figure 1 shows, the Auger and TA spectra are in a good agreement in the ankle region (from $10^{18.4}$ eV to $\simeq 10^{19.4}$ eV), when the Auger energies are increased by +5.2% and the TA energies are reduced by 5.2%. Such shifts are well within the stated uncertainties in the energy scales of both experiments. A large difference remains above $\simeq 10^{19.5}$ eV, in the region of the suppression.

The sources of differences in the energy scales of both experiments, as well as the exposure and resolution unfolding calculations, have been cross-checked in the UHECR-2014 meeting. In the WG report of UHECR-2016, and in this work, we focus on the remaining difference in the region of the high energy suppression. To determine whether this difference is an instrumental or an astrophysical effect, we have performed a comparison of Auger and TA spectra in the *common declination band*, a range of declination values that is in the field of view of both experiments: $-15.7^\circ < \delta < 24.8^\circ$. In this work, we use the Auger and TA analyses with upper limits on the event zenith angles of 60° and 55° , respectively. Moreover, for the purposes of this comparison, we use a new spectrum calculation technique that takes into account the details of the Auger and TA exposure dependence on the declination [3].

3. Comparison of the TA and Auger spectra in the common declination band

Figure 2 shows the directional exposures of the two experiments. For the Auger vertical anal-

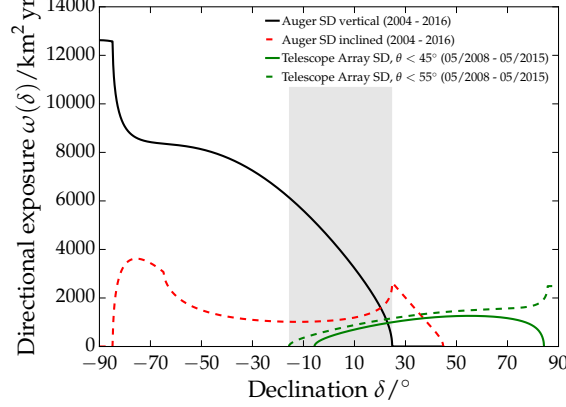


Figure 2: Auger and TA exposure plotted versus declination. For Auger, shown are the exposure values for the vertical (black solid line) and inclined (dashed red line) analyses. For TA, the exposure is shown for the maximum zenith angle cuts of 45° (green solid line) and 55° (green dashed line). Gray shaded area shows the TA and Auger common declination band, which extends from -15.7° to 24.8°.

ysis that covers declinations from -90° to 24.8°, the total exposure is 51,588 km² sr yr. For TA analysis with event zenith angles extending to 55°, the total exposure is 8,300 km² sr yr. TA is sensitive in the declination range from -16° to 90°.

In order to calculate and compare the Auger and TA spectra in the common declination band (shaded area in Figure 2), we use the following method:

$$J_{1/\omega}(E) = \frac{1}{\Delta\Omega\Delta E} \sum_{i=1}^N \frac{1}{\omega(\delta_i)} \quad (3.1)$$

where $J_{1/\omega}(E)$ is the differential flux J as a function of energy E , calculated by this "1/ω - method", $\Delta\Omega = 2\pi \int_{\delta_{\min}}^{\delta_{\max}} d\delta \cos(\delta)$ is the solid angle covered by the common declination band ($\delta_{\min} = -15.7^\circ$, $\delta_{\max} = 24.8^\circ$), ω is the directional exposure shown in Figure 2, and δ_i is the declination of the i^{th} event. The sum is over N events in the energy interval ΔE . The statistical uncertainty of $J_{1/\omega}(E)$, if one were to ignore any anisotropies, is given by (to first order):

$$\Delta J_{1/\omega}(E) = \frac{1}{\Delta\Omega\Delta E} \left\{ \frac{\int_{\delta_{\min}}^{\delta_{\max}} d\delta \cos(\delta) / \omega(\delta)}{\int_{\delta_{\min}}^{\delta_{\max}} d\delta \omega(\delta) \cos(\delta)} \right\}^{1/2} \sqrt{N} \quad (3.2)$$

For the formal derivation of this method, as well as the cross-checks with the standard TA and Auger spectrum calculation techniques, please see [3]. The Left panel of Figure 3 shows the results with Auger and TA energies scaled by $\pm 5.2\%$ (as in the right panel of Figure 1). When we fit the two results, $J_{1/\omega}^{\text{Auger}}$ and $J_{1/\omega}^{\text{TA}}$, to broken power law functions, the high energy cutoff points become only 0.6 σ different: $\log_{10}(E/\text{eV}) = 19.59 \pm 0.04$ for TA, and $\log_{10}(E/\text{eV}) = 19.56 \pm 0.03$ for

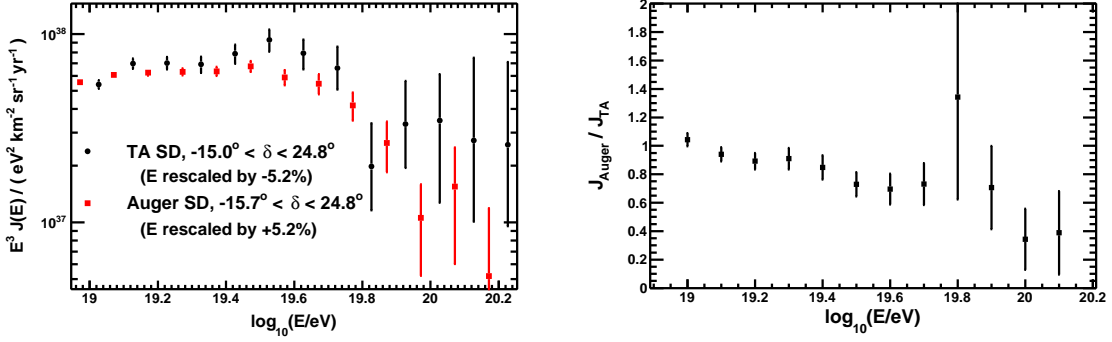


Figure 3: Left: Auger SD (red squares) and the TA SD (black circles) spectra in the common declination band, calculated using the $1/\omega$ method. The Auger energy scale has been increased by 5.2% while the TA energies have been decreased by 5.2%, as it was done in the right panel of Figure 1. Right: Ratio of the Auger (J_{Auger}) and TA (J_{TA}) fluxes that have been calculated using the $1/\omega$ method.

Auger. This agreement is an important step towards comparing the results of the two experiments. However, differences still remain, as it can be seen in the right panel of the Figure 3: the ratio of fluxes $J_{1/\omega}^{\text{Auger}}/J_{1/\omega}^{\text{TA}}$, in the common declination band, depends on energy in a significant way.

We have also examined possible declination dependencies of the spectra within each individual experiment. In the case of Auger, as Figure 4 shows, the spectrum does not appear to depend on the declination in a significant way. All three Auger spectra, for declinations $-90^\circ < \delta <$

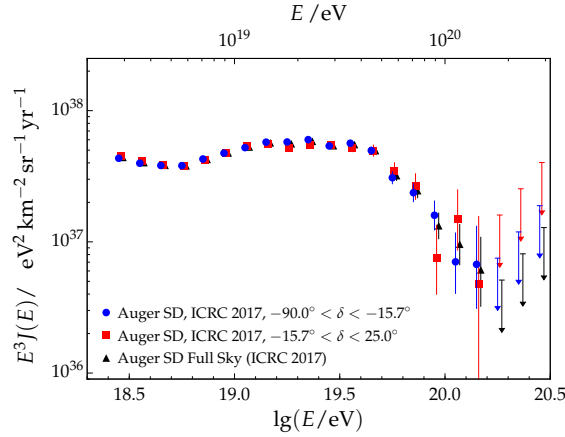


Figure 4: Auger spectra covering the sky to the south of the common declination band (shown in blue), common declination band (shown in red), and the combination of the two (shown in black).

-15.7° , $-15.7^\circ < \delta < 25.0^\circ$, and $-90.0^\circ < \delta < 25.0^\circ$, are in a good agreement among each other. In the case of TA, on the other hand, the situation is different: as Figure 5 shows, the break point (using the broken power law fit) in the spectrum for lower declinations $-16^\circ < \delta < 24.8^\circ$ occurs at $\log_{10}(E/\text{eV}) = 19.59 \pm 0.06$, while for $24.8^\circ < \delta < 90^\circ$, the second break point occurs at $\log_{10}(E/\text{eV}) = 19.85 \pm 0.03$. It should be noted that although the spectrum calculations in

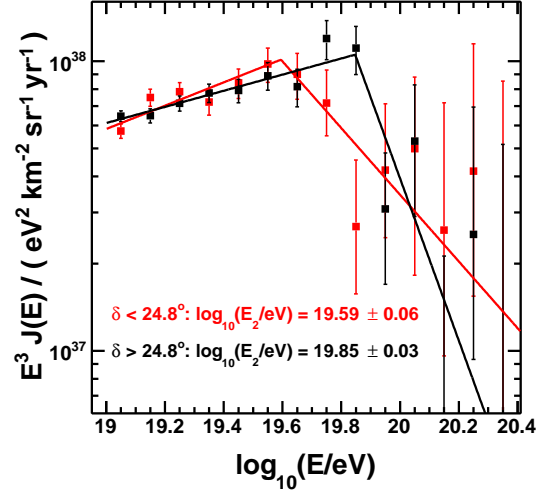


Figure 5: TA surface detector spectra for two declination bands: common declination band (in red) and over the rest of the northern hemisphere (in black).

Figures 4, 5 used traditional Auger and TA methods, cross-checks have been made [8, 9], and it was shown that the $1/\omega$ method produced similar results [3].

4. Summary

We have reviewed and compared the results of the UHECR spectra measured by the Pierre Auger and Telescope Array experiments. It was established that scaling the energies of Auger and TA by +5.2% and -5.2%, respectively, brings the two measurements into a good agreement around the ankle region from $10^{18.4}$ eV to $\simeq 10^{19.4}$ eV. Energy scaling of 5.2% is well within the systematic uncertainties stated by the experiments. At the energies around the suppression region, on the other hand, we have found that even after restricting the comparison to the region of the sky that is observed by both experiments, despite a noticeable improvement in the agreement of the spectra, statistically significant differences were still present. We have not identified the sources of the remaining discrepancies at this time.

References

- [1] B.R. Dawson *et al.*, for the Telescope Array and Pierre Auger Collaborations, *EPJ Web of Conferences* **53** (2013) 01005.
- [2] I. Mariş *et al.*, for the Telescope Array and Pierre Auger Collaborations, talk given at the 2014 Conference on Ultrahigh Energy Cosmic Rays, Springdale, Utah (USA).
- [3] T. AbuZayyad *et al.*, for the Telescope Array and Pierre Auger Collaborations, proceedings of the 2016 Conference on Ultrahigh Energy Cosmic Rays, Kyoto (Japan).
- [4] The Pierre Auger Collaboration, *Nucl. Instrum. Meth. A* 798 (2015) 172.
- [5] T. Abu-Zayyad *et al.*, *Nucl. Instrum. Meth. A* 689 (2013) 87.
- [6] T. Abu-Zayyad *et al.*, *Nucl. Instrum. Meth. A* 676 (2012) 54.
- [7] T. Abu-Zayyad *et al.*, *Astropart. Phys.* **109** (2012) 39.
- [8] F. Fenu, for the Pierre Auger Collaboration, these proceedings.
- [9] D. Ivanov, for the Telescope Array Collaboration, these proceedings.



Testing the agreement between the X_{\max} distributions measured by the Pierre Auger and Telescope Array Observatories

Vitor de Souza^{*a} for the Pierre Auger Collaboration^b and the Telescope Array Collaboration^c

^a*Instituto de Física de São Carlos, Universidade de São Paulo, São Paulo, Brazil*

^b*Observatorio Pierre Auger, Av. San Martín Norte 304, 5613 Malargüe, Argentina*

E-mail: auger_spokespersons@fnal.gov

Full author list: http://www.auger.org/archive/authors_icrc_2017.html

^c*Telescope Array Project, 201 James Fletcher Bldg, 115 S. 1400 East, Salt Lake City, UT 84112-0830, USA*

E-mail: ta-icrc@cosmic.utah.edu

Full author list: <http://www.telescopearray.org/research/colaborators>

The Auger-TA composition working group reports on a comparison of X_{\max} distributions measured by the Pierre Auger and Telescope Array Observatories. The shapes of the X_{\max} distributions measured by the Auger and TA Observatories are evaluated and a quantitative compatibility test is presented. A direct comparison of the measured X_{\max} distributions is not correct due to different detector acceptances and resolutions as well as different analysis techniques. In this contribution, a method developed to allow a correct comparison of the X_{\max} distributions is explained and used. A set of showers compatible to the composition measured by the Auger detectors was simulated and reconstructed using the official TA software chain. This procedure simulates an energy-dependent composition mixture, which represents a good fit to Auger X_{\max} distributions, exposed through the detector acceptance, resolution and analysis procedure of the TA experiment. Two compatibility tests are applied to the X_{\max} distributions: Kolmogorov-Smirnov and Anderson-Darling. Both tests show that TA data is within the systematic uncertainties compatible to a mixed composition such as the one measured by the Auger detectors.

*35th International Cosmic Ray Conference — ICRC217
10–20 July, 2017
Bexco, Busan, Korea*

^{*}Speaker.

1. Introduction

The mass composition is a crucial ingredient in our understanding of Ultra-High Energy Cosmic-Rays (UHECR) origin and production mechanism. The complete UHECR puzzle can only be solved on the basis of a reliable composition measurement. The depth at which air-showers reach their maximum energy deposit (X_{\max}) correlates with the primary particle mass [1]. The fluorescence measurement technique was developed to measure X_{\max} with good resolution [2] and extract the mass composition from a sample of showers. The construction of the next generation of fluorescence telescopes [3, 4] and new analysis procedures brought the technique to a high standard level. Today X_{\max} can be measured with a resolution better than 25 g/cm^2 by Auger and TA Observatories.

The work presented here is a comparison of the X_{\max} distributions measured by the Auger and TA Observatories in the energy range from $10^{18.2}$ to 10^{19} eV. The energy range of this study is limited to $E < 10^{19}$ eV due to the lack of events in TA's data above this energy. The TA collaboration wishes to understand better what is the potential effect of under-sampling bias in energy bins with small statistics.

A direct comparison of the X_{\max} distributions and its moments as published by both collaborations is wrong because of the different detector resolutions, acceptance and analysis procedures. The acceptance and biases of fluorescence telescopes depend on X_{\max} and therefore the raw distribution of measured shower maxima is always biased by detector effects. Each collaboration (Auger and TA) chose a different analysis procedure to deal with the particularities of the fluorescence technique. Therefore no conclusion about possible discrepancies between Auger and TA composition measurements is possible when a comparison is based directly on the published results of both collaborations.

In the next sections, a procedure to pass the composition which best fits the Auger X_{\max} measurements¹ through the official TA simulation, reconstruction and analysis chain is described. This method imposes the TA resolution, acceptance and biases onto the AUGERMIX. This is the only way to compare the X_{\max} results of both collaborations and therefore to make conclusions about possible discrepancies. This method was already applied to the first moment of the distribution ($\langle X_{\max} \rangle$) and presented at the ICRC2015 [7] and UHECR2016 [8] conferences. The comparison showed that the mean of the distributions measured by the Auger and TA collaborations are in agreement within the systematic uncertainties. No discrepancy is seen in the mean of the X_{\max} distributions when the proper comparison is done.

In this contribution, the same method is applied to the entire X_{\max} distribution. The argument and the conclusion of previous studies based on the moments of distribution is valid for a detailed analysis of the full distribution. A quantitative comparison of the X_{\max} distributions is done after the simulation of the AUGERMIX composition through the TA detectors and analysis chain. No discrepancy is found between the TA data and AUGERMIX composition. In other words, within the systematic uncertainties, the TA data is compatible to the composition measured by the Auger detectors. The details of the analysis are shown in the next sections.

¹The composition which best fits the Auger X_{\max} distributions is named AUGERMIX from now on.

2. Main differences of the analysis procedures used by the Pierre Auger and TA Collaborations

The analysis strategies used by the collaborations are different from the start. The Pierre Auger Collaboration elaborated an analysis procedure aimed on minimizing detection and reconstruction bias such as to publish the moments of the X_{\max} distributions as close as possible to the true values [5]. The TA collaboration elaborated an analysis procedure using minimal cuts. This maximizes available statistics, and the published data has detection and reconstruction biases. These are dealt with by carefully simulating the detector in MC and comparing the biased data to similarly biased MC simulations [6].

Figure 1 illustrates the effect of the differences in analysis and detectors in the X_{\max} distribution measured by the two experiments. The black line in the figure represents a fit of a X_{\max} distribution for proton shower simulated with Conex [9] and QGSJetII-04 [10] hadronic interaction model. This sample of simulated showers was passed through the Auger and TA detector simulation and analysis chains. The green distribution represent the X_{\max} distribution that would be published by the TA collaboration if this pure proton composition impinged the detector. The orange distribution represents the X_{\max} distribution that would be published by the Auger collaboration if this pure proton composition impinged the detector. These two distributions are clearly different due to differences in the analysis strategies. This example illustrates why a direct comparison of the published X_{\max} distributions and their moments is not possible. The number of events in the orange (green) distribution is 814 (311) according to the number of events published by each collaboration in this energy range. The first and second moments of the Simulation, Auger and TA distributions are 766.6, 764.6, 760.9 and 63.3, 60.9, 58.4 g/cm², respectively.

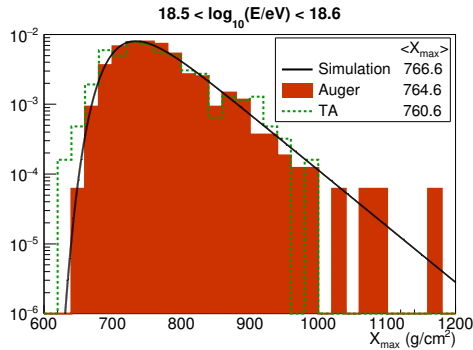


Figure 1: Illustration of Auger and TA analysis strategies. Black line corresponds to proton simulation (Conex [9] and QGSJetII-04 [10]). Green distribution represents these simulated showers as reconstructed by the TA. The orange distribution represents this simulated showers as reconstructed by the Auger.

The Auger Collaboration publishes X_{\max} values (X_{\max}^{Auger}) different from values published by the TA Collaboration X_{\max}^{TA} due to particular treatment of biases and detector efficiency. A proper comparison of the published data is only possible if detector simulation is used to convert X_{\max}^{Auger} to X_{\max}^{TA} . In the next section, a method to convert X_{\max}^{Auger} as measured by Auger to X_{\max}^{TA} as measured by TA is explained². Only after a proper conversion of the quantities, is it possible to draw conclusions about the compatibility of the two data sets.

3. Method to compare X_{\max} measurements done by the Pierre Auger and TA Observatories

Ultimately it would be desirable to have the Auger and TA detectors running side-by-side for a certain period of time measuring the same air showers. This would lead to the best cross-

² X_{\max}^{TA} : AUGERMIX simulated through TA telescopes and analysis chain.

calibration of the detectors and an event-by-event comparison of the reconstructed values. Since this is not possible, simulations were done to mimic TA detection of events with an Auger-like mass composition.

The procedure starts by using the model developed to describe the X_{\max}^{Auger} data as published in reference [11]. In this study, the X_{\max}^{Auger} distributions were fit using simulated air showers from different primary nuclei. The study varied the flux of four primary particles and calculated the mix of elements which best describes the X_{\max}^{Auger} distributions. Figure 2 shows the fraction of each primary that best describes Auger data when the QGSJETII-04 hadronic interaction model is used. The composition which best describes Auger data in the energy range from $10^{18.2}$ to $10^{19.0}$ eV is a mix of Proton, Helium and Nitrogen nuclei which is named as AUGERMIX. In this paper, the fit of the Auger data done with QGSJetII-04 is used for illustration. The same calculations were repeated with the EPOS-LHC [12] hadronic interaction model and the same conclusion on the compatibility of the TA and Auger X_{\max} distributions was reached.

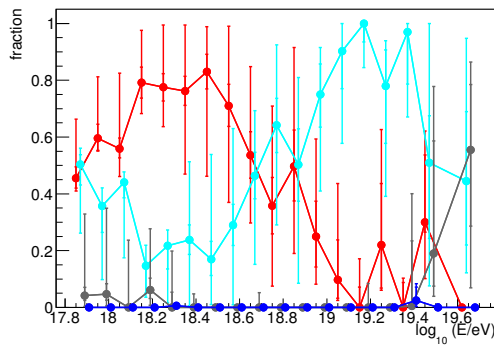


Figure 2: Fraction of primary nuclei which best describes X_{\max} distributions measured by Auger when fitted with QGSJetII-04. Red, cyan, gray and blue corresponds to Pr, He, N and Fe nuclei, respectively. Statistical (smaller) and systematic (larger) uncertainties are shown. Points were shifted in x-axis for clarity. Only $18.2 < \log_{10}(E/\text{eV}) < 19.0$ is used in this paper.

The AUGERMIX is simulated thought the TA detectors using the official simulation package of the TA Collaboration. The simulated events are analyzed using the same procedure applied for the data measured by the TA telescopes. The result of this exercise is the transformation of the AUGERMIX into $_{\text{Auger}}X_{\max}^{\text{TA}}$. Figure 3 shows the distributions of $_{\text{TA}}X_{\max}^{\text{TA}}$ (X_{\max} distributions as published by TA including detector resolution and acceptance) and $_{\text{Auger}}X_{\max}^{\text{TA}}$ (X_{\max} distributions that would be published by TA if a mix composition of showers equivalent to the one measured by the Auger detectors (AUGERMIX) impinged the TA detectors).

4. Comparison of X_{\max} distributions

The distributions in figure 3 can now be compared directly because they both include the biases and efficiency of the TA detectors. Two tests of compatibility of distributions were used: Kolmogorov-Smirnov and Anderson-Darling (see e.g. [13]). The Kolmogorov-Smirnov (KS) test is one of the most used compatibility procedures used in the literature with a response enhanced near the peak of the distribution. The Anderson-Darling (AD) test is optimized to probe differences in the tails of the distributions. Both tests calculate the probability (P1) that two distributions were generated by the same parent distribution. The probability calculated that $_{\text{TA}}X_{\max}^{\text{TA}}$ and $_{\text{Auger}}X_{\max}^{\text{TA}}$ are generated from the same parent distribution is named P1^{data} .

In order to normalize these probabilities and extract a measure of compatibility, a distribution of compatible P1 was generated by the following procedure. The $_{\text{Auger}}X_{\max}^{\text{TA}}$ distributions were fitted by a Gaussian convoluted with a exponential function [14]. One hundred thousand distributions

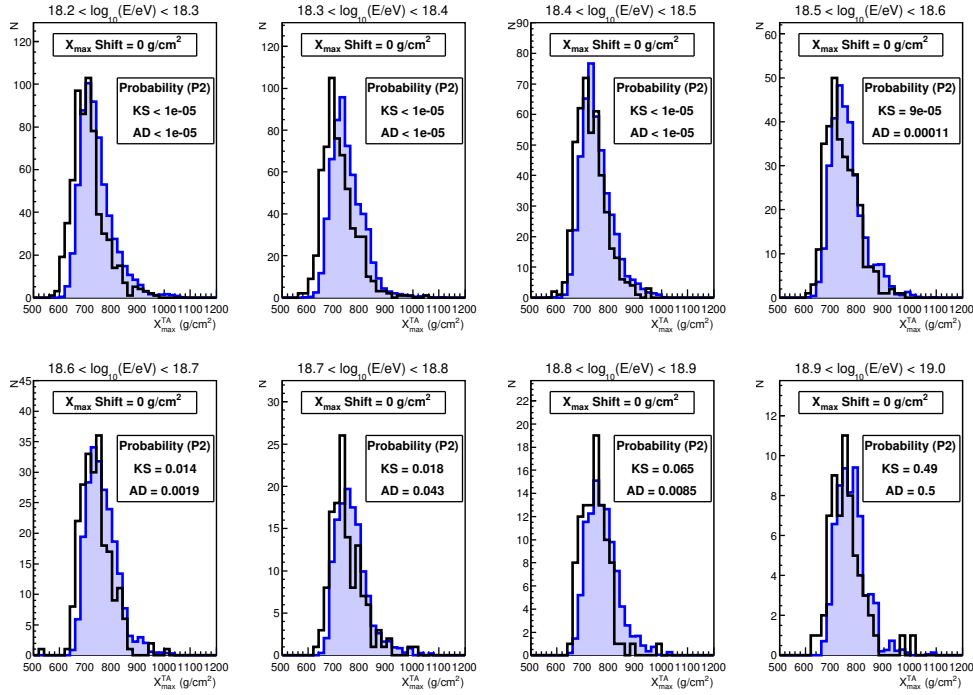


Figure 3: X_{\max}^{TA} distributions. Black is TA data and blue is AUGERMIX simulated thought the TA detector and reconstruction chain ($\text{Auger}X_{\max}^{TA}$). For each energy bin the value of P1 and P2 are shown as defined in section 4.

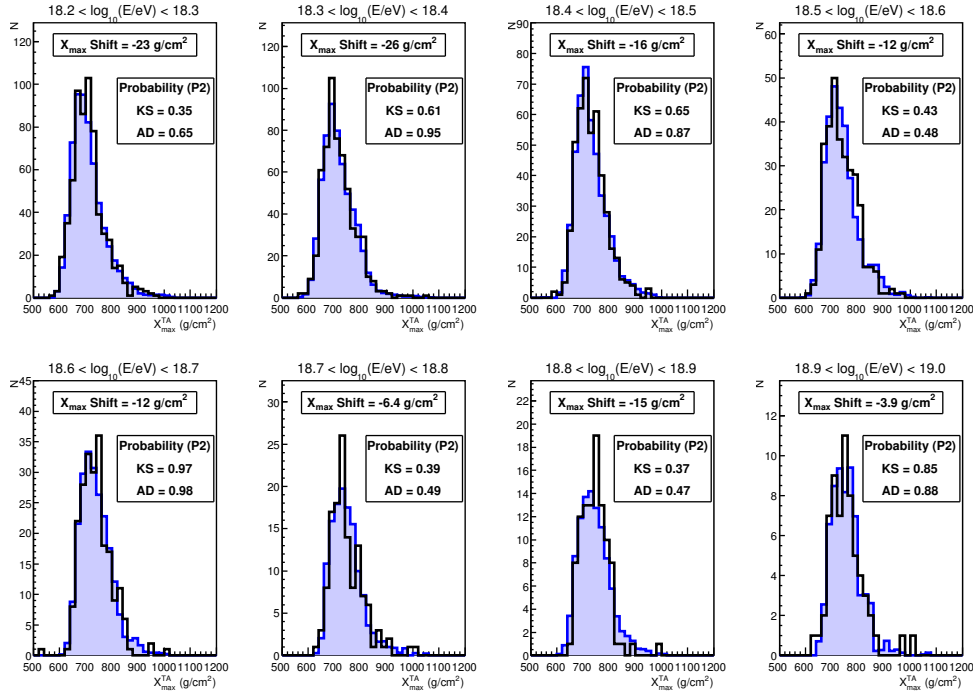


Figure 4: X_{\max}^{TA} distributions. Black is TA data and blue is AUGERMIX simulated thought the TA detector and reconstruction chain ($\text{Auger}X_{\max}^{TA}$). For each energy bin the value of P1 and P2 are shown as defined in section 4. The shift in X_{\max} ($\langle X_{\max}^{TA} \rangle - \langle \text{Auger}X_{\max}^{TA} \rangle$) done to match the distributions mean is also shown.

of $_{\text{Auger}}X_{\max}^{\text{TA}}$ were randomly generated from the fitted function using standard Monte Carlo (MC) techniques. Each MC $_{\text{Auger}}X_{\max}^{\text{TA}}$ distribution had the same number of events as $_{\text{TA}}X_{\max}^{\text{TA}}$ distributions, i.e. the number of events measured by TA detectors. The P1 probability that the original $_{\text{Auger}}X_{\max}^{\text{TA}}$ distribution and each MC $_{\text{Auger}}X_{\max}^{\text{TA}}$ distribution was calculated ($P1^{\text{MC}}$). Figure 5 shows an example of the $P1^{\text{MC}}$ distribution. Given that MC $_{\text{Auger}}X_{\max}^{\text{TA}}$ distributions were generated from the original $_{\text{Auger}}X_{\max}^{\text{TA}}$ distribution, figure 5 shows the distribution of P1 for compatible distributions.

Finally, the compatibility probability (P2) between $_{\text{TA}}X_{\max}^{\text{TA}}$ and $_{\text{Auger}}X_{\max}^{\text{TA}}$ is given by the probability to find $P1^{\text{MC}}$ larger than $P1^{\text{data}}$. In other words, P2 measures the probability to find in a random set of distributions generated from $_{\text{Auger}}X_{\max}^{\text{TA}}$, a distribution as compatible as $_{\text{TA}}X_{\max}^{\text{TA}}$ and $_{\text{Auger}}X_{\max}^{\text{TA}}$. Typically values of P2 larger than 0.01 express large probability of compatibility between the distributions. Table 1 (column “No X_{\max} shift”) shows the P2 values as a function of energies corresponding to the distributions in figure 3. The values of P2 in the studied energy shows a general incompatibility of the distributions for energies below $10^{18.6}$ eV, a marginal compatibility for $18.6 < \log_{10}(E/\text{eV}) \leq 18.9$ and a good agreement in the last energy bin $18.9 < \log_{10}(E/\text{eV}) \leq 19.0$ eV ($P2_{\text{KS}} = 0.49$ and $P2_{\text{AD}} = 0.5$).

If the distributions are allowed to be shifted by the systematic uncertainties quoted by the Auger and TA collaborations the agreement gets evidently better. Figure 4 show the distributions shifted to have the same mean. Table 1 (column “ X_{\max} shift”) shows the results of the compatibility analysis. $_{\text{Auger}}X_{\max}^{\text{TA}}$ distributions were shifted by the values shown in the figure to match the mean of $_{\text{TA}}X_{\max}^{\text{TA}}$ distributions. Figure 6 shows the comparison of the values by which $_{\text{Auger}}X_{\max}^{\text{TA}}$ distributions were shifted with the sum of the systematic uncertainties of both experiments. The Auger Collaboration quotes systematic uncertainties as a function energy [5] of about $\pm 8 \text{ g/cm}^2$ and the TA Collaboration quotes systematic uncertainties of $\pm 20.3 \text{ g/cm}^2$ [8].

Figure 7 shows the P2 values between $_{\text{TA}}X_{\max}^{\text{TA}}$ and $_{\text{Auger}}X_{\max}^{\text{TA}}$ distributions after the shift (TA \leftrightarrow AUGERMIX). The values of P2 show a very good agreement between $_{\text{TA}}X_{\max}^{\text{TA}}$ and $_{\text{Auger}}X_{\max}^{\text{TA}}$ distributions. As a reference, the same comparison was data using instead of the AUGERMIX a pure proton composition (TA \leftrightarrow Proton). The same level of agreement between the TA data and proton is seen between TA data and the AUGERMIX composition.

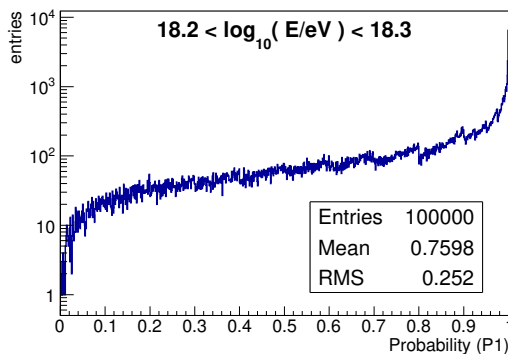


Figure 5: Example of a distribution of $P1^{\text{MC}}$ for the Anderson-Darling test.

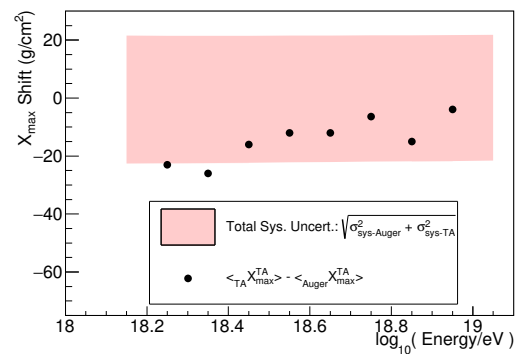


Figure 6: Comparison of the shift in X_{\max} with the systematic uncertainty in X_{\max} .

Energy bin $\log_{10}(E/\text{eV})$	Compatibility Probability (P2)							
	No X_{\max} shift		X_{\max} shift $\langle X_{\max}^{\text{TA}} \rangle - \langle X_{\max}^{\text{Auger}} \rangle$					
	KS	AD	TA \leftrightarrow AUGERMIX			TA \leftrightarrow Pr		
			Shift (g/cm^2)	KS	AD	Shift (g/cm^2)	KS	AD
18.2 - 18.3	$< 10^{-5}$	$< 10^{-5}$	-23	0.35	0.65	-31	0.14	0.21
18.3 - 18.4	$< 10^{-5}$	$< 10^{-5}$	-26	0.61	0.95	-33	0.99	0.99
18.4 - 18.5	$< 10^{-5}$	$< 10^{-5}$	-16	0.65	0.87	-22	0.57	0.62
18.5 - 18.6	9×10^{-5}	1.1×10^{-4}	-12	0.43	0.48	-21	0.41	0.53
18.6 - 18.7	0.014	0.0019	-12	0.97	0.98	-24	0.92	0.95
18.7 - 18.8	0.018	0.043	-6.4	0.39	0.49	-20	0.67	0.88
18.8 - 18.9	0.065	0.0085	-15	0.37	0.47	-31	0.55	0.26
18.9 - 19.0	0.49	0.5	-3.9	0.85	0.88	-20	0.98	0.98

Table 1: Compatibility probability between the X_{\max}^{TA} and X_{\max}^{Auger} and between X_{\max}^{TA} and pure proton distributions as defined by two methods: Kolmogorov-Smirnov (KS) and Anderson-Darling (AD). See section 4 for details about P2.

5. Conclusion

In this paper, a) Monte Carlo simulation of air-showers, b) simulation of the TA detectors and c) the TA reconstruction and analysis chain were used to produce the X_{\max} distributions that would be published by the TA collaboration in case a mixed composition that describes the X_{\max} distributions measured by the Auger detectors impinged the TA detectors. This method converts the X_{\max} measurement done by Auger in the X_{\max} measurements done by TA.

Throughout this paper, X_{\max}^{Auger} refers to X_{\max} distributions which best describes the Auger data simulated and analyzed through the TA detectors. X_{\max}^{TA} refers to the X_{\max} distributions published by TA which includes the detector and analysis effects. The plots presented were done using the best description of the Auger data when analyzed with the QGSJetII-04 hadronic interaction. The complete study was repeated using the best description of the Auger data when analyzed with the EPOS-LHC hadronic interaction model. The conclusions presented below do not depend on the hadronic interaction model used to describe the Auger data.

A direct comparison of X_{\max}^{Auger} and X_{\max}^{TA} is the only way to quantify possible discrepancies between the two data sets measured by the Auger and TA. Direct comparison of the results published by each collaboration independently is not possible. Interpretations of UHECR composition involving Auger and TA results should refer to the results presented here and in previous conferences [7, 8] as agreed by both collaborations.

Two quantitative compatibility tests were applied to X_{\max}^{Auger} and X_{\max}^{TA} distributions: Kolmogorov-Smirnov and Anderson-Darling. The methods are complementary because these focus on the peak (KS) or tails (AD) of the distributions respectively. The compatibility tests show very good agreement between X_{\max}^{Auger} and X_{\max}^{TA} distributions within the systematic uncertainties.

The conclusion of the study presented here is that the X_{\max} data measured by TA is compatible to a mixed composition which best describes the Auger X_{\max} data. No significant departure from

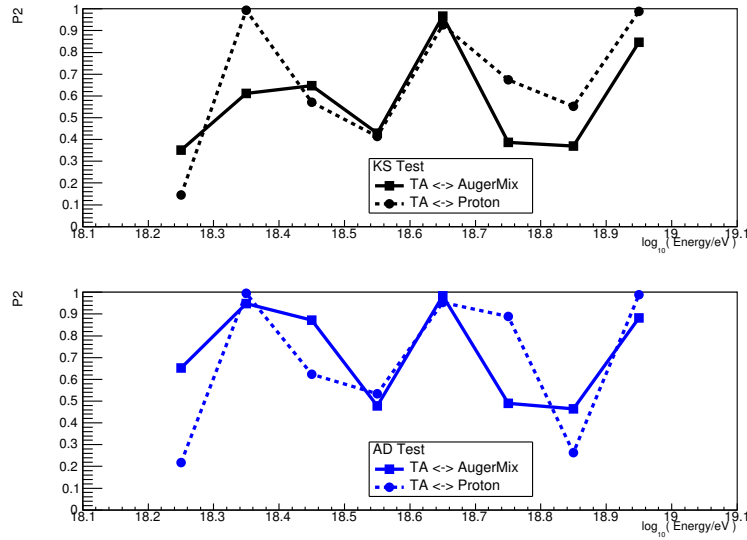


Figure 7: Compatibility probability between the $TA X_{\max}^{TA}$ and $Auger X_{\max}^{TA}$ distributions as defined by two methods: Kolmogorov-Smirnov (KS) and Anderson-Darling (AD). See section 4 for details about P2.

the hypothesis that both distributions were generated from the same parent distribution was found. At the current level of statistics and understanding of systematics, the TA data is consistent with the proton models used in this paper for energies less than 10^{19} eV and it is also consistent with the AUGERMIX composition as described above. More TA data is needed to confirm the trend to a heavier composition seen in Auger data above $\sim 10^{19}$ eV.

References

- [1] J. Matthews, *Astroparticle Physics*, 22 (2005) 387.
- [2] The High Resolution Fly’s Eye Collaboration, *The Astrophysical Journal*, 622 (2005) 910.
- [3] The Pierre Auger Collaboration, *NIM A* 620 (2010) 227-251.
- [4] The Telescope Array Collaboration, *NIM A*, 676 (2012) 54.
- [5] The Pierre Auger Collaboration, *Physical Review D* 90, 122005 (2014).
- [6] The Telescope Array Collaboration, *Astroparticle Physics* 64 (2015) 49.
- [7] M. Unger for the Pierre Auger and TA Collaborations, ICRC 2015, page 10, arXiv 1511.02103.
- [8] W. Hanlon for the Pierre Auger and TA Collaborations, UHECR Conference 2016.
- [9] T. Bergmann et al., *Astroparticle Physics*, 26 (2007) 420.
- [10] S. Ostapchenko, *Physical Review D*, 83 (2011) 014018.
- [11] The Pierre Auger Collaboration, *Physical Review D* 90, 122006 (2014).
- [12] T. Pierog et al., *Physical Review C*, 92 2015, 034906.
- [13] Frank Porter, arXiv 0804.0380.
- [14] C.J.T. Peixoto et al., *Astroparticle Physics* 47 (2013) 18.